

Abstract of thesis entitled

# This is the title of my thesis

Submitted by

**Cheuk Yee LO**

for the degree of Doctor of Philosophy  
at The University of Hong Kong  
in August 2018

These are the motivations. These are the methods. These are the results.  
These are the discussions. These are the significance.

---

*An abstract of exactly 499 words*

# **This is the title of my thesis**

by

**Cheuk Yee LO**

A thesis submitted in partial fulfilment of the requirements for  
the Degree of Doctor of Philosophy  
at The University of Hong Kong.

August 2018

# **Declarations**

I declare that this thesis represents my own work, except where acknowledgement is made, and that it has not been previously included in a thesis, dissertation or report submitted to this University or to any other institution for a degree, diploma or other qualifications.

Signed .....  
.....

Cheuk Yee LO

# Acknowledgments

This command generate dummy text. Remove this line and replace it by your words of appreciation.

# Contents

<b>Abstract</b>	i
<b>Title Page</b>	ii
<b>Declaration</b>	iii
<b>Acknowledgments</b>	iv
<b>Contents</b>	v
<b>List of Figures</b>	viii
<b>List of Tables</b>	x
<b>List of Abbreviations and Symbols</b>	xi
<b>1 Theoretical Background</b>	1
1.1 Introduction . . . . .	1
1.2 Standard Model . . . . .	1
1.2.1 Matter particles . . . . .	2
1.2.2 Forces and carrier particles . . . . .	3
1.2.3 Feynman diagram . . . . .	3
1.3 Limitation of Standard Model . . . . .	3
1.3.1 Dark matter . . . . .	3
1.3.2 Hierarchy problem . . . . .	5
1.3.3 Unification of forces . . . . .	6
1.4 Supersymmetry . . . . .	6
1.4.1 Minimal Supersymmetric Standard Model . . . . .	7
1.5 Wh channel . . . . .	7

<b>2 Experimental Setup</b>	<b>8</b>
2.1 Introduction . . . . .	8
2.2 The Large Hadron Collider . . . . .	8
2.3 ATLAS detector . . . . .	10
2.3.1 coordinate system . . . . .	12
2.3.2 magnetic system . . . . .	12
2.3.3 The inner detector . . . . .	12
2.3.4 Calorimeter . . . . .	17
2.3.5 Muon Spectrometer . . . . .	17
<b>3 Dataset inputs and event selection</b>	<b>18</b>
3.1 Dataset inputs . . . . .	18
3.1.1 Data samples . . . . .	18
3.1.2 MC samples . . . . .	19
3.2 Pre-selection and event cleaning . . . . .	20
<b>4 Pre-selection</b>	<b>22</b>
4.1 Trigger selection . . . . .	22
4.2 Event selection . . . . .	22
4.3 Object definitions . . . . .	22
4.3.1 electrons and muons . . . . .	22
4.3.2 jets . . . . .	22
4.3.3 Missing transverse energy . . . . .	22
<b>5 Signal Region</b>	<b>23</b>
<b>6 Background estimation</b>	<b>24</b>
6.1 charge flip background . . . . .	24
6.1.1 Sources for charge flip background . . . . .	24
6.1.2 Likelihood method . . . . .	26
6.1.3 Background subtraction . . . . .	28
6.1.4 Results without systematic uncertainty . . . . .	28
6.1.5 Systematic uncertainties due to background subtraction . . . . .	30
6.1.6 Systematic uncertainties due to likelihood method . . . . .	30
6.1.7 Results with total uncertainties . . . . .	32
6.1.8 MC validation . . . . .	33

6.2	fake lepton background . . . . .	35
6.2.1	Sources for fake lepton background . . . . .	35
6.2.2	Matrix method . . . . .	36
6.2.3	Measurement of real efficiencies . . . . .	40
<b>7</b>	<b>Validation regions</b>	<b>41</b>
<b>A</b>	<b>List of MC samples</b>	<b>42</b>
A.1	List of background MC samples . . . . .	42
A.2	List of signal MC samples . . . . .	46
<b>References</b>		<b>49</b>

# List of Figures

1.1	The table for all fundamental particles in SM. [1]	2
1.2	All allowed fundamental Feynman vertices in SM, except higgs-related vertices. [2]	4
1.3	All allowed fundamental higgs-related Feynman vertices in SM.	5
2.1	The schematic diagram of the CERN accelerator complex, which shows a series of accelerators and facilities. [3]	9
2.2	The cut-away view of the ATLAS detector. It is 25m high and 44m long. [4]	11
2.3	The cross section of the ATLAS detector. This shows different components of the ALTAS and how ATLAS detect different types of particles [5]	11
2.4	The whole structure of the ATLAS inner detector. [6]	13
2.5	The distances R from the beam for the 3 components: pixel, SCT and TRT. [6]	14
2.6	The shapes, the orientations and the $\eta$ coverage for each sensor. [7]	15
2.7	whole calorimeter [8]	16
2.8	muon spectrometer [9]	17
6.1	This shows how the track of the electron is incorrectly reconstructed (the orange track), due to the process of bremsstrahlung and $\gamma$ conversion.	25
6.2	This shows how the track of the electron is incorrectly reconstructed (the orange track), due to very high $p_T$ of the electron.	25
6.3	The measured values of the charge-flip rate $\epsilon_i$ in data. Only uncertainties due to the likelihood method are included.	29

6.4	The systematic variations of the charge-flip rate $\epsilon_i$ in data, due to the background subtraction. . . . .	31
6.5	This diagram shows how the original electron is found through the decay chain. . . . .	31
6.6	The comparison between the likelihood method and the MC truth method, by using the $Z \rightarrow ee$ MC samples. Hence, the systematic uncertainties due to likelihood method can be estimated. . . . .	33
6.7	The measured values of the charge-flip rate $\epsilon_i$ in data, with total uncertainties. . . . .	34
6.8	The comparison between the weighted OS events and the SS events, with different variables. . . . .	35

# List of Tables

6.1	Binning in $p_T$ and $ \eta $ for the charge-flip rate $\epsilon_i$ .	26
A.1	List of simulated W+jets processes	42
A.2	List of simulated Z+jets processes	43
A.3	List of simulated single-top processes	43
A.4	List of the simulated $t\bar{t}$ sample	43
A.5	List of simulated $t\bar{t}$ plus vectorboson processes	43
A.6	List of simulated higgs related processes, including Higgs plus vector boson production and $t\bar{t}H$ processes	44
A.7	List of simulated diboson processes	44
A.8	List of simulated triboson processes	44
A.9	List of simulated drellyan processes	44
A.10	List of simulated multi-top processes	44
A.11	List of simulated V+ $\gamma$ processes	45
A.12	List of signal samples	47

# List of Abbreviations and Symbols

LHC Large Hadron Collider

SUSY Supersymmetry

# Chapter 1

## Theoretical Background

### 1.1 Introduction

Particle physics is a branch of physics that studies the most fundamental particles and their interaction. We believe that all matter and radiation in the universe are made up of these fundamental particles, and their behaviour is described by the theories in particle physics. In 20th century, our understanding about the nature of fundamental particles has had great breakthrough and advance. Also, many particle colliders have been built to give much insight to develop the theories and test the theories. The currently mainstream theory of particle physics is called the Standard Model.

### 1.2 Standard Model

Standard Model(SM) is the current theory to describe the fundamental particles in particle physics. It has already gained huge success in predicting the experimental results, including the prediction of existence of the top quark, the tau neutrino, and the Higgs boson. It has also explained almost all experimental results with high accuracy. It represents our best understanding of how the fundamental particles interact with each other.

Physicists discovered that there are 4 fundamental force in the universe: electromagnetic force, weak force, strong force, and gravitational force. However, SM can only describe 3 of them: electromagnetic, weak and strong interaction, and the gravity cannot be described by SM. Figure 1.1 shows all fundamental particles in SM, and their mass, electric charge and spin. All matter is made up of

# Standard Model of Elementary Particles

three generations of matter (fermions)					
	I	II	III		
mass	$\approx 2.4 \text{ MeV}/c^2$	$\approx 1.275 \text{ GeV}/c^2$	$\approx 172.44 \text{ GeV}/c^2$	0	$\approx 125.09 \text{ GeV}/c^2$
charge	2/3	2/3	2/3	0	0
spin	1/2	1/2	1/2	1	0
	u	c	t	g	H
	up	charm	top	gluon	Higgs
QUARKS	$\approx 4.8 \text{ MeV}/c^2$	$\approx 95 \text{ MeV}/c^2$	$\approx 4.18 \text{ GeV}/c^2$	0	$\approx 125.09 \text{ GeV}/c^2$
	-1/3	-1/3	-1/3	0	0
	1/2	1/2	1/2	1	0
	d	s	b	$\gamma$	photon
	down	strange	bottom		
	$\approx 0.511 \text{ MeV}/c^2$	$\approx 105.67 \text{ MeV}/c^2$	$\approx 1.7768 \text{ GeV}/c^2$	0	$\approx 91.19 \text{ GeV}/c^2$
	-1	-1	-1	1	1
	1/2	1/2	1/2	Z	Z boson
	e	$\mu$	$\tau$		
LEPTONS	$<2.2 \text{ eV}/c^2$	$<1.7 \text{ MeV}/c^2$	$<15.5 \text{ MeV}/c^2$	0	$\approx 80.39 \text{ GeV}/c^2$
	0	0	0	1	1
	1/2	1/2	1/2	W	W boson
	$\nu_e$	$\nu_\mu$	$\nu_\tau$		
	electron neutrino	muon neutrino	tau neutrino		
SCALAR BOSONS					
GAUGE BOSONS					

Figure 1.1: The table for all fundamental particles in SM. [1]

fermions (purple and green), which is the first 3 columns in figure 1.1. Fermions are divided into two groups: quarks(purple) and leptons(green). The forces between the fermions are mediated by the force carriers, which is gauge bosons(red). Higgs bosons(yellow) is scalar bosons, which give mass to other massive particles.

## 1.2.1 Matter particles

There are 6 types of quarks: up quarks(u), down quarks(d), charm quarks(c), strange quarks(s), top quarks(t) and bottom quarks(b). Quarks interacts with strong interaction, while leptons does not. There are 3 types of charged leptons: electrons, muons and taus. There are 3 types of neutral leptons: electron neutrinos, muon neutrinos and tau neutrinos. The first column is the first generation, which is the lightest and most stable particles. Hence, normal matter in our daily life is made from the particles in the first generation. The second and third col-

umn are the second and third generation respectively, which is heavier and less stable particles. These particles will finally decay into the particles in the first generation. Due to the phenomenon of neutrino oscillation, neutrinos should have non-zero masses, but their value are still uncertain in our current technology.

### 1.2.2 Forces and carrier particles

Photon is the force carrier for electromagnetic interaction. Gluon is the force carrier for strong interaction. Z and W boson is the force carrier for weak interaction. The effects of these fundamental forces stem from the exchange of the corresponding force carrier. These forces also have different strengths and different ranges. Strong force is the strongest force, while the electromagnetic force is in the middle. The weak force is the weakest force among the three, but it still much much stronger than the gravity. The electromagnetic force has infinite range, while the strong and weak forces have very short ranges at the level of subatomic particles.

For example, a proton is composed of two up quarks and one down quark, and a neutron is composed of one up quark and two down quarks. The forces between quarks inside the proton are mediated by gluons.

### 1.2.3 Feynman diagram

The fundamental interactions among these fundamental particles are described by the allowed fundamental Feynman vertices. All allowed fundamental Feynman vertices in SM are shown in figure 1.2 and 1.3. These fundamental vertices are the basic building blocks for all physical processes, by jointing these vertices together.

## 1.3 Limitation of Standard Model

Although Standard Model can explain almost all experimental results, there still are some phenomena it cannot explain.

### 1.3.1 Dark matter

Dark matter is some unknown matter that does not involve in electromagnetic interaction, but involve in gravitational interaction. It was first discovered in the Milky Way, by studying the speed of the stars orbiting around the center of the Milky Way. Because it does not involve in electromagnetic interaction, it does

## Standard Model Interactions (Forces Mediated by Gauge Bosons)

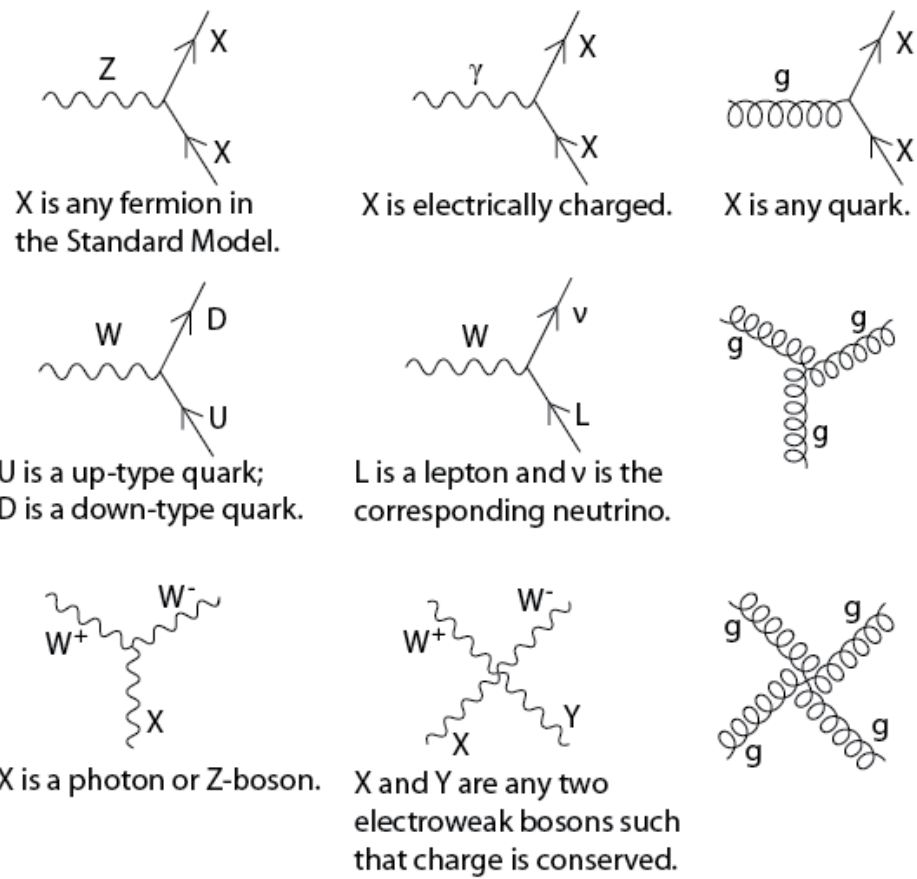


Figure 1.2: All allowed fundamental Feynman vertices in SM, except higgs-related vertices. [2]

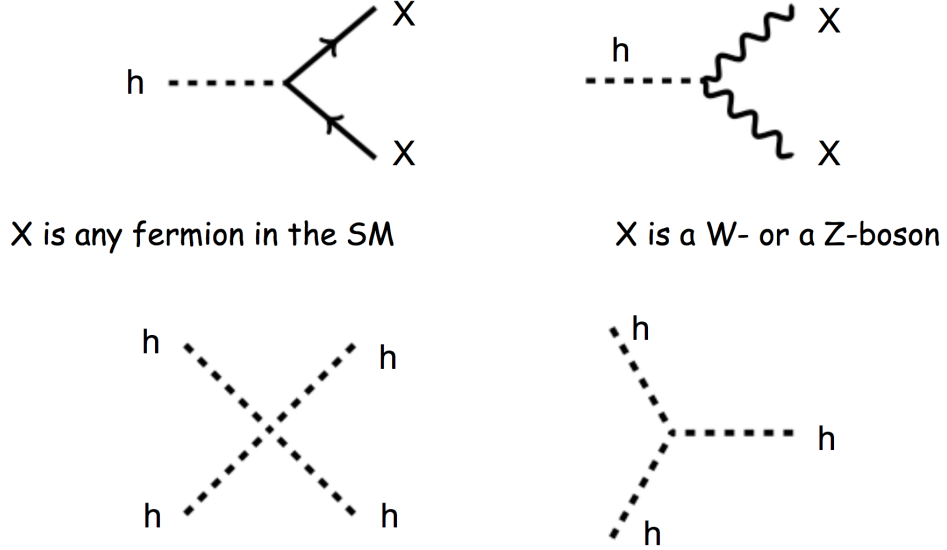


Figure 1.3: All allowed fundamental Higgs-related Feynman vertices in SM.

not emit any electromagnetic radiation, and it cannot be seen by our telescopes. However, SM cannot explain the nature of dark matter, and what dark matter is made of.

### 1.3.2 Hierarchy problem

The hierarchy problem is the question why the weak force is stronger than the gravitational force by  $10^{24}$  times. It is also asked why the mass of Higgs boson ( $\sim 125$  GeV) is much lighter than the Planck mass ( $\sim 10^{19}$  GeV).

The Lagrangian for the interaction term between the fermion Dirac field  $\psi$  and the Higgs field  $h$  (i.e. Yukawa interaction) is given by

$$\mathcal{L}_{\text{Yukawa}} = -\lambda \bar{\psi} h \psi \quad (1.1)$$

where  $\lambda$  is the Yukawa coupling constant. The quantum correction to the square of the Higgs mass  $\Delta m_H^2$  is then given by

$$\Delta m_H^2 = -\frac{|\lambda|^2}{16\pi^2} \Lambda^2 + \dots \quad (1.2)$$

where  $\Lambda$  is the energy scale up to which the Standard Model is valid, namely the Planck scale ( $\sim 10^{19}$  GeV). Because  $\Lambda$  is quadratic divergent, the correction to the Higgs mass is in the order of Planck scale. Unless there are very delicate cancellation between the correction terms, the Higgs mass should be in the order

of Planck scale. But, we found that the experimental Higgs mass is in the order of 125 GeV, and this is called the hierarchy problem.

### 1.3.3 Unification of forces

In the 1860s, James Clerk Maxwell wrote down his famous equations Maxwell's equations, which unified two different phenomena: electricity and magnetism. Due to this unification, we now understand that electricity and magnetism are two different manifestations of the same phenomenon, and we now call it electromagnetism.

Similar thing happened in 1970s, physicists developed a theory that unified two fundamental forces: electromagnetic force and weak force. At the energy scale above 246 GeV, these two forces will merge into a single force: electroweak force. This unification predicted the existence of weak neutral current and a force carrier to carry this weak force. This force carrier was later confirmed experimentally in CERN, and it is now called the Z boson.

After that, an effect of strong force was found experimentally that the strong force becomes weaker when the energy is higher. This may indicate that electroweak force and strong force will become a single force at even high energy. However, the energy scale at which these forces are the same is much larger than the energy the particle accelerators can reach. There are some theories beyond the Standard Model that try to unify these force, such as supersymmetry.

## 1.4 Supersymmetry

Supersymmetry(SUSY) is an extension of the Standard Model, and try to answer some questions which the Standard Model cannot explain mentioned in section 1.3. One of the problem SUSY can solve is the hierarchy problem of Higgs mass mentioned in section 1.3.2. We first notice that the negative sign in the equation 1.2 is due to the correction from the fermions. If we can somehow have some symmetry between the fermions and bosons, and add more positive correction terms due to the bosons, the correction terms will cancel with each other and the hierarchy problem can be solved. This new symmetry is called the supersymmetry(SUSY).

#### **1.4.1 Minimal Supersymmetric Standard Model**

Minimal Supersymmetric Standard Model(MSSM) is the minimal supersymmetrical theory that contain the least number of new particle states and new interactions. It predicts that each particle in the Standard Model has its own partner particle, called the superpartner. The name of the superpartner is by adding a prefix "s", followed by the name of the orginal Standard Model particle. For example, the superpartner of an electron is called selectron. As for the symbol for the superpartner, a tilde will be added above the original symbol. For example, the symbol for selectron is  $\tilde{e}$ . Also, the spin of the superpartner will differ from the Standard Model particle by 1/2. For fermions, the spin of their superpartner is 0, while for bosons, the spin of their superpartner is 1/2. This is the new symmetry between the fermions and bosons, mentioned before. It is also the correction terms from these superpartners to fix the hierarchy problem of the Higgs mass. If MSSM is correct, these supersymmetric particles should be detected in the LHC.

### **1.5 Wh channel**

# Chapter 2

## Experimental Setup

### 2.1 Introduction

Our experimental data was collected from the ATLAS particle detector in the Large Hadron Collider (LHC). The following section will introduce LHC and the ATLAS particle detector.

### 2.2 The Large Hadron Collider

The Large Hadron Collider (LHC) was built in the border between France and Switzerland by the European Organization for Nuclear Research (CERN). It is a circular particle collider under the ground with circumference 27 km. Two beams of protons will be accelerated in opposite directions, to almost the speed of light, and then these two beams will collide with each other at the collision point. The energy of each beam is 6.5 TeV, and hence the center-of-mass energy of the two beams  $\sqrt{s}$  is 13 TeV, which is the energy used in this experiment. This energy is equivalent to the speed that the beam will circulate the ring 11,245 times per second. Under this high energy, new physics phenomena will happen, including SUSY. Figure 2.1 shows the schematic diagram of the CERN accelerator complex, which contains a series of accelerators, from low energy to high energy. The dark blue big circle in figure 2.1 represents the LHC, on which there are 4 particle detectors at 4 different interaction points (yellow points): ATLAS, CMS, LHCb and ALICE. By analyzing these collisions, we can have a deeper understanding of the laws of nature.

Before the beam is injected into LHC, the protons need to be accelerated by a

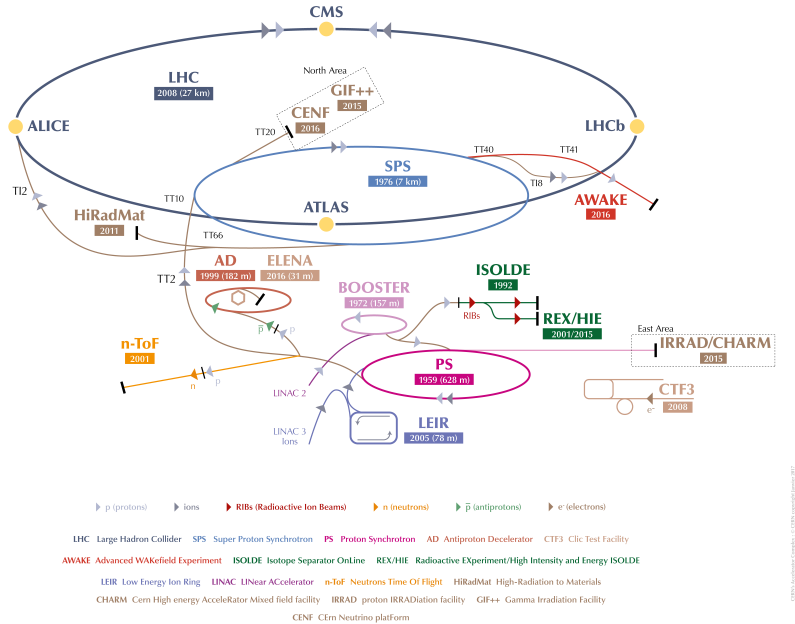


Figure 2.1: The schematic diagram of the CERN accelerator complex, which shows a series of accelerators and facilities. [3]

series of accelerators. The journey of the protons starts from a tank of hydrogen gas. The proton and the electron are separated by a electric field. The protons are then accelerated to 50 MeV by Linac2, which is a linear accelerator. The beam is then injected to the second accelerator called the Proton Synchrotron Booster (PSB), which accelerates the beam to 1.4 GeV. The beam is then injected to the third accelerator called the Proton Synchrotron (PS), which pushes the beam to 25 GeV. The beam is then injected to the fourth accelerator called the Super Proton Synchrotron (SPS), which further pushes the beam to 450 GeV. Finally, the beam is injected to the two beam pipes of the LHC. One of the beam moves in clockwise direction, while another beam moves in anti-clockwise direction. Two beams will be collided at the collision point inside the ATLAS detector. [10]

The circular path of the proton beam is maintained by many superconducting electromagnets along the LHC tunnel. There are 1232 main magnetic dipoles, and each of them generates a large magnetic field of 8.3 T. In order to generate such a high magnetic field, the coils need to have very high current of 11,080 A, and hence superconducting coil need to be used, to reduce the heat loss due to the electrical resistance. The material of superconducting coil is niobium-titanium

(NbTi). To reach the condition for superconductivity, the electromagnets operate at a very low temperature of 1.9 K. There are also 392 magnetic quadrupole to squeeze the proton beam, so that the chance of proton-proton collision will be higher. [11, 12]

The protons in the beam are grouped into different bunches, and there are about  $10^{11}$  protons in each bunch. The time-spacing between two adjacent bunches is 25ns (or 50 ns in the old configuration). This means that in each 25 ns, two bunches are collided at the collision point. For each bunch collision, there are about 10 to 50 proton-proton interaction. Hence, about  $10^9$  proton-proton collisions are produced in one second.

The interacting rate for a physics process  $\frac{dN}{dt}$  is the product of the cross section of that physics process  $\sigma$  and the instantaneous luminosity  $\mathcal{L}$ .

$$\frac{dN}{dt} = \sigma \mathcal{L} \quad (2.1)$$

The instantaneous luminosity  $\mathcal{L}$  is a measure of the interacting rate of two protons at the collision point, which is related to the density of the protons and the speed of the protons. The instantaneous luminosity in this experiment is about  $10^{34}$   $\text{cm}^{-2} \text{s}^{-1}$  (or  $10 \text{ nb}^{-1} \text{s}^{-1}$ ).

## 2.3 ATLAS detector

A Toroidal LHC ApparatuS (ATLAS) is the particle detector used in this experiment [7]. Figure 2.2 shows the main components of the ATLAS detector. The ATLAS detector is a general purpose particle detector, which is consisted of 3 main components: the inner detector, the calorimeter and the muon spectrometer. Figure 2.3 shows how the ATLAS distinguishes different types of particle. The inner detector can detect the paths of the charged particles. Photons and electrons will deposit most of their energy in the electromagnetic calorimeter, and finally stop by it. Hadrons(including protons and neutrons) and mesons will similarly stop by the hadronic calorimeter. Only muons and the neutrinos can reach the outermost muon spectrometer, but only muons can be detected by the muon spectrometer. Nearly all neutrinos will escape the whole ATLAS detector, which leads to some missing energy. In this design, different particles can be identified due to their signature in different parts of ATLAS.

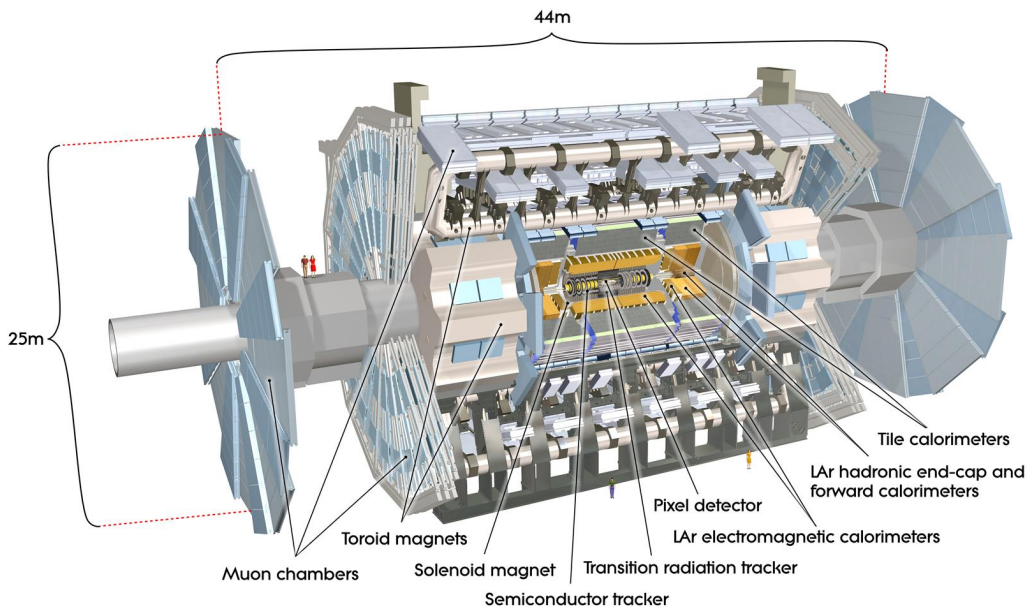


Figure 2.2: The cut-away view of the ATLAS detector. It is 25m high and 44m long. [4]

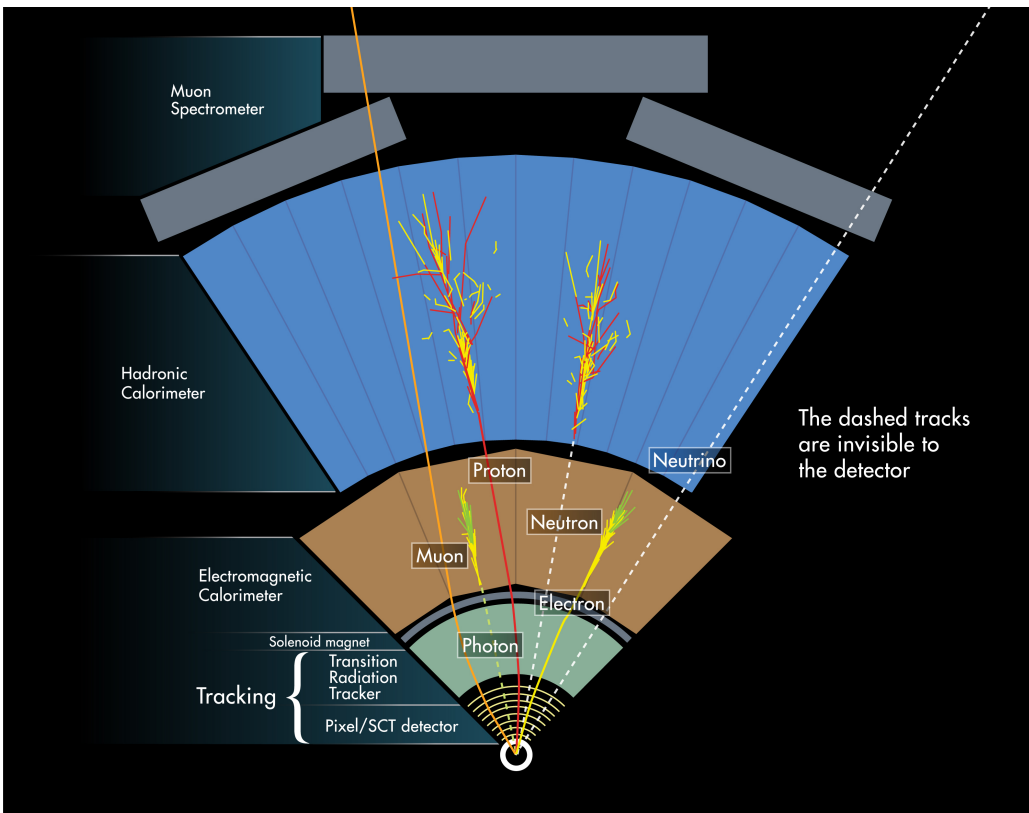


Figure 2.3: The cross section of the ATLAS detector. This shows different components of the ALTAS and how ATLAS detect different types of particles [5]

### 2.3.1 coordinate system

The nominal collision point is defined as the origin of the coordinate system. The z-axis is along the beam direction. The positive x-axis is pointing to the centre of the LHC ring. The positive y-axis is in the upward direction. The azimuthal angle  $\phi$  and the polar angle  $\theta$  are defined as usual in the spherical coordinate system. The pseudorapidity  $\eta$  is defined as:

$$\eta = -\ln \left( \tan \frac{\theta}{2} \right) \quad (2.2)$$

The distance  $\Delta R$  in the pseudorapidity-azimuthal angle space is defined as:

$$\Delta R = \sqrt{(\Delta\phi)^2 + (\Delta\eta)^2} \quad (2.3)$$

The ATLAS detector has a reflection symmetry about the x-y plane.

### 2.3.2 magnetic system

There is a thin superconducting solenoid magnet around the inner detector, which generates a 2 T magnetic field inside the inner detector. There are also 3 large superconducting toroids around the calorimeter: one for barrel and two for end-caps. All these magnets are shown in figure 2.2.

### 2.3.3 The inner detector

The inner detector is a particle tracker. It mainly detects the tracks of charged particles and has good performance for measuring the momentum of the charged particles and locating the position of the vertices. Figure 2.4 shows the whole structure of the inner detector. The inner detector consists of 3 sub-detectors from inner to outer: the pixel detector, the silicon microstrip tracker (SCT) and the transition radiation tracker (TRT). Each part further divides into two parts: the barrel region with smaller  $|\eta|$  and the end-cap region with larger  $|\eta|$ . Figure 2.5 shows the distances  $R$  from the beam for the 3 sub-detectors, and figure 2.6 shows the shapes and the orientations of each sensor and the  $\eta$  coverage, in both the barrel and the end-cap regions. The  $\eta$  coverage for the inner detector is  $|\eta| < 2.5$ . The shapes and the orientations of the sensors are different in the barrel and the end-cap regions. In the barrel region, the shape and the orientation of the sensors is concentric cylinder shells around the beam axis, while in the end-cap region, they are disks perpendicular to the beam axis.

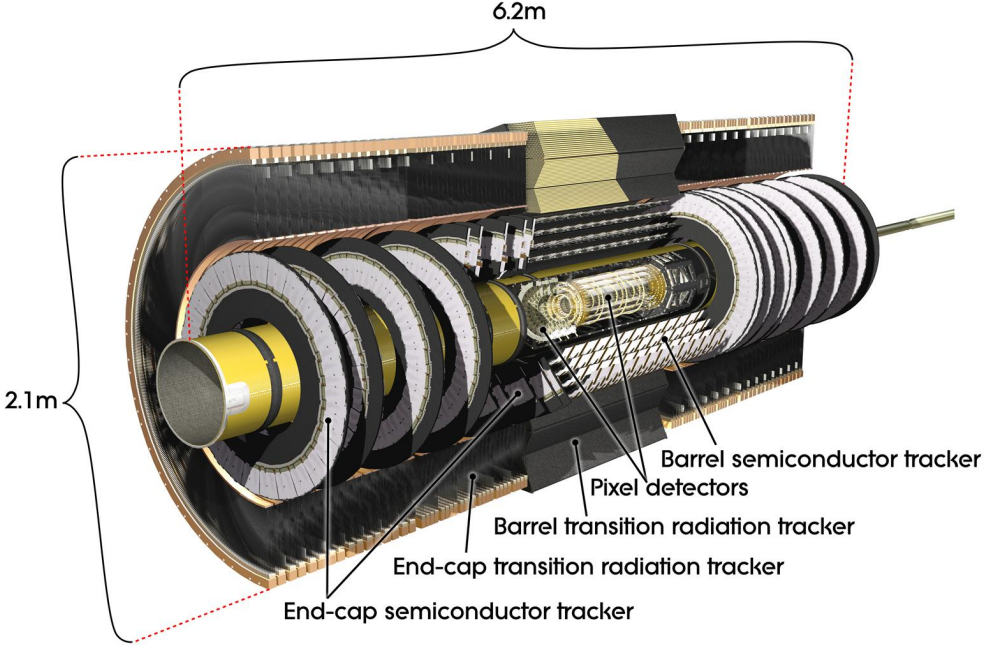


Figure 2.4: The whole structure of the ATLAS inner detector. [6]

The precision tracking detectors (pixels and SCT) has high resolution in space by using discrete space-points to detect the track of a charged particle, with the cutting-edge technology, in order to achieve the good performance of the inner detector. When the particle moves inside the inner detector, there are, in average, 36 hits per one track. By recording the positions of these hits, the path of the particle can be reconstructed. The whole inner detector is immersed in a 2 T magnetic field generated by the solenoid magnet, and hence the path of any charged particles will be bent. By measuring the curvature of the path, the charge and momentum of the particle can be measured. The equation for the circular path is

$$\frac{d\mathbf{p}}{dt} = q(\mathbf{v} \times \mathbf{B}) \quad (2.4)$$

where the relativistic momentum  $\mathbf{p} = \gamma m\mathbf{v}$ .

$$\frac{d\mathbf{p}}{dt} = q\left(\frac{\mathbf{p}}{\gamma m} \times \mathbf{B}\right) \quad (2.5)$$

$$= \frac{q}{\gamma m}(\mathbf{p} \times \mathbf{B}) \quad (2.6)$$

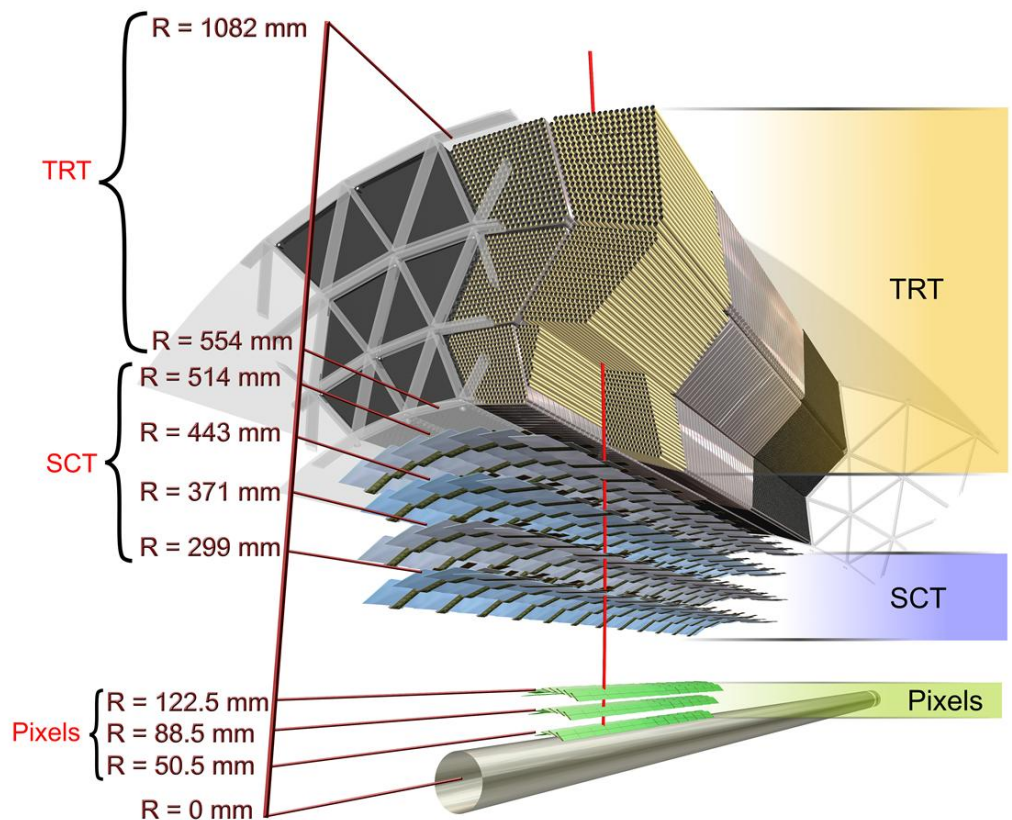


Figure 2.5: The distances  $R$  from the beam for the 3 components: pixel, SCT and TRT. [6]

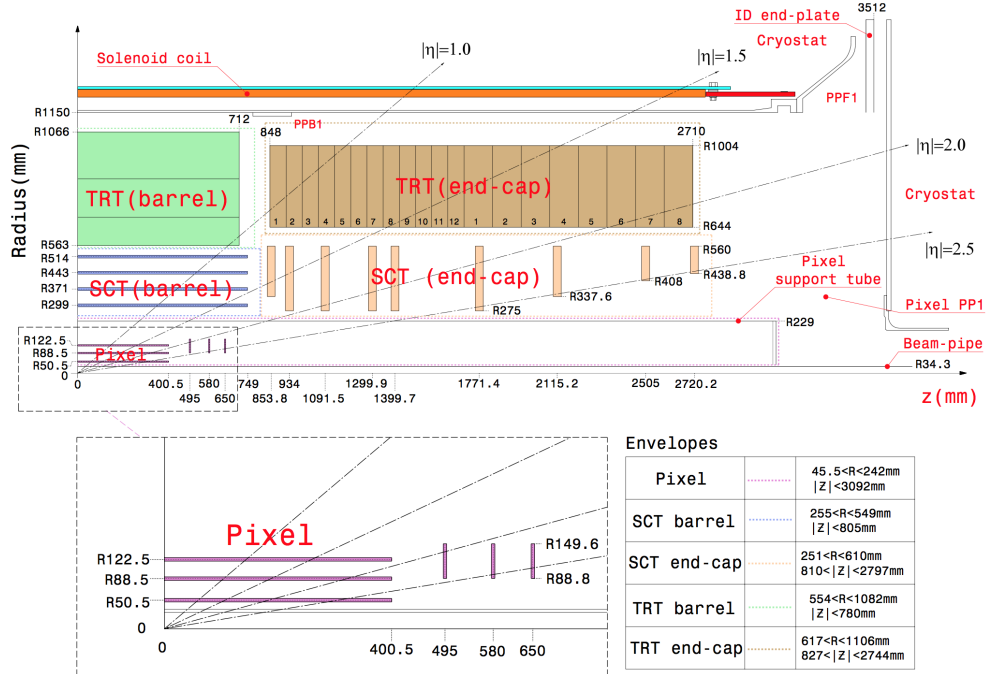


Figure 2.6: The shapes, the orientations and the  $\eta$  coverage for each sensor. [7]

From this equation, we can get the angular frequency  $\omega$ ,

$$\omega = \frac{qB}{\gamma m} \quad (2.7)$$

$$\frac{v}{r} = \frac{qB}{\gamma m} \quad (2.8)$$

$$\frac{1}{r} = \frac{qB}{\gamma mv} \quad (2.9)$$

$$\frac{1}{r} = \frac{qB}{p} \quad (2.10)$$

$$p = rqB \quad (2.11)$$

By this equation, we can calculate the momentum of the particle, from the curvature of track  $1/r$ , the charge and the magnetic field strength.

### 2.3.3.1 Pixel detector

As shown in figure 2.6, there are 3 layers of cylinder in the barrel region, and 3 layers of disk for each end-cap region. There are in total 1744 modules in the pixel detectors. Each module is identical, and has the size of  $19\text{mm} \times 63\text{mm}$ , and  $250\ \mu\text{m}$  thick. The module has 47232 pixels, which has size of  $50\mu\text{m} \times 400\mu\text{m}$ , and hence there are in total 80 million pixels for the whole pixel detector. Each pixel has the accuracy of  $10\mu\text{m} \times 115\mu\text{m}$ . The sensor is using planar n<sup>+</sup>-in-n type of

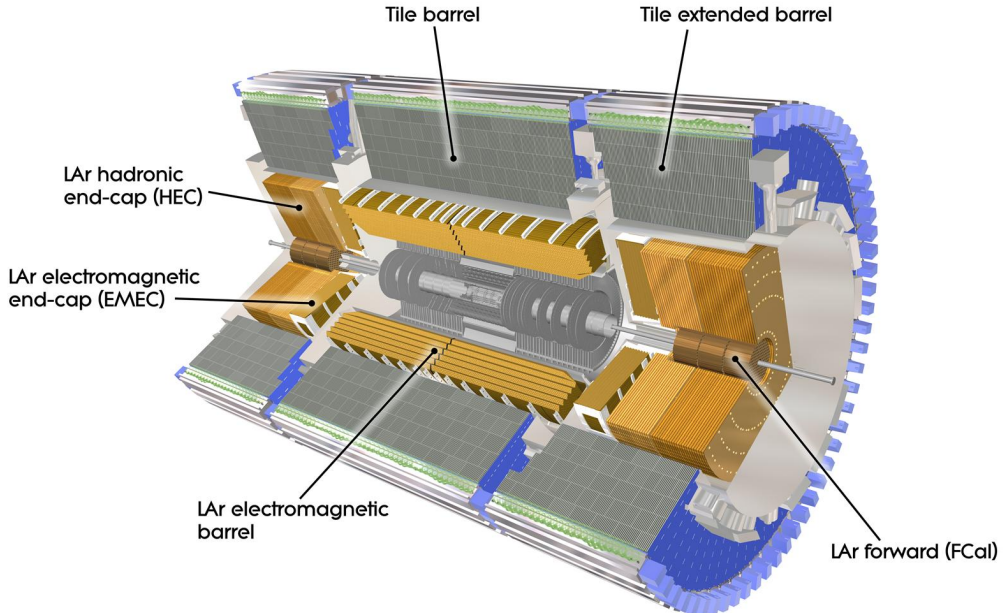


Figure 2.7: whole calorimeter [8]

silicon, with  $n^+$ -type at the readout side and n-type at another side.

### 2.3.3.2 SCT

As shown in figure 2.6, there are 4 layers of cylinder in the barrel region, and 9 layers of disk for each end-cap region. There are in total 4088 modules in the SCT, with the thickness of  $285\ \mu m$ . There are in total 6.3 million pixels for the SCT. Each pixel has the accuracy of  $17\mu m \times 580\mu m$ . The sensor is using planar p-in-n type of silicon.

### 2.3.3.3 TRT

136 TRT modules. TRT in the outer part is to produce and detect the transition radiation from the particle. TRT comprises many layers of gaseous straw tube elements interleaved with transition radiation material. Each pixel has the accuracy of  $130\mu m$ .

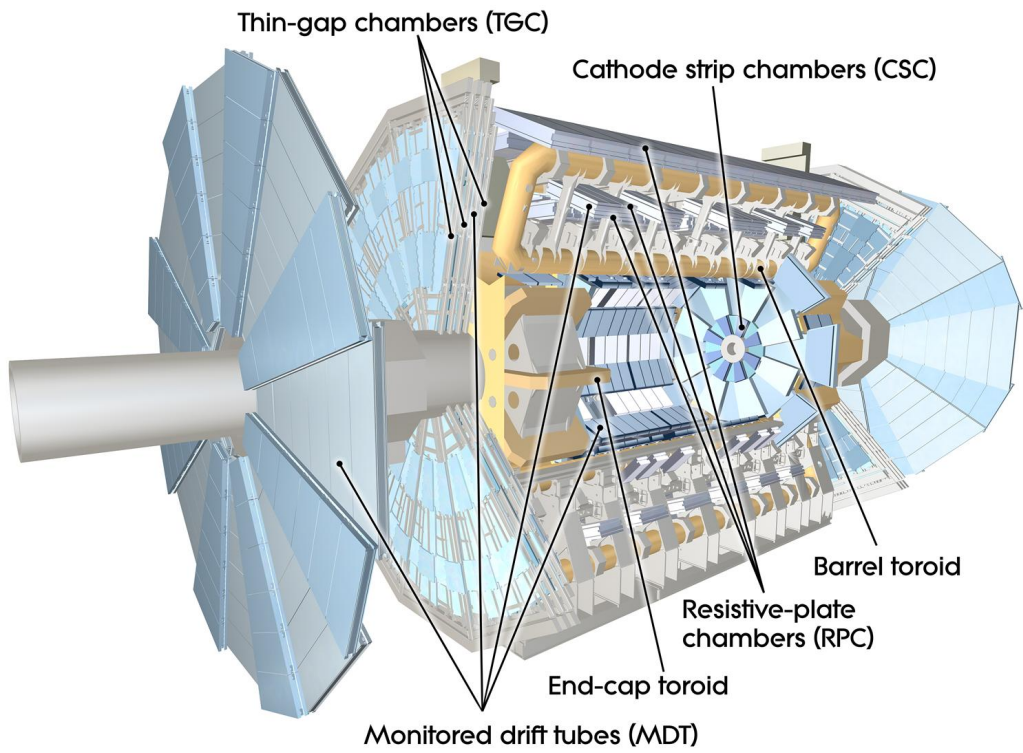


Figure 2.8: muon spectrometer [9]

### 2.3.4 Calorimeter

#### 2.3.4.1 Electromagnetic calorimeter

#### 2.3.4.2 Hardronic calorimeter

### 2.3.5 Muon Spectrometer

# Chapter 3

## Dataset inputs and event selection

### 3.1 Dataset inputs

This chapter describes the dataset used in this analysis. The dataset contains the data samples and Monte-Carlo(MC) simulated sample. All dataset are SUSY2 DxAOD derivations, which aim for 2 or 3 leptons search.

#### 3.1.1 Data samples

We use 2015 (periods D-H and J) and 2016 (period A-L, I, K and L)  $pp$ -collisions data samples, at  $\sqrt{s} = 13$  TeV. Only events with good condition are used, where LHC beams were stable and all ATLAS detectors were in good state. The following two Good Run Lists (GRL) describe what events is used in 2015 and 2016 data.

- `data15_13TeV.periodAllYear_DetStatus-v79-repro20-02_DQDefects-00-02-02_PHYS_StandardGRL--All_Good_25ns.xml` for 2015 data.
  
- `data16_13TeV.periodAllYear_DetStatus-v89-pro21-01_DQDefects-00-02-04_PHYS_StandardGRL--All_Good_25ns.xml` for 2016 data.

The integrated luminosities in 2015 and 2106 are  $3.21\text{ fb}^{-1}$  and  $32.86\text{ fb}^{-1}$  respectively, with relative error 2.1%. The following are the list of data samples used.

```
data15_13TeV.periodD.physics_Main.PhysCont.DAOD_SUSY2.grp15_v02_p2950
data15_13TeV.periodE.physics_Main.PhysCont.DAOD_SUSY2.grp15_v02_p2950
data15_13TeV.periodF.physics_Main.PhysCont.DAOD_SUSY2.grp15_v02_p2950
data15_13TeV.periodG.physics_Main.PhysCont.DAOD_SUSY2.grp15_v02_p2950
```

```

data15_13TeV.periodH.physics_Main.PhysCont.DAOD_SUSY2.grp15_v02_p2950
data15_13TeV.periodJ.physics_Main.PhysCont.DAOD_SUSY2.grp15_v02_p2950
data16_13TeV.periodA.physics_Main.PhysCont.DAOD_SUSY2.grp16_v02_p2950
data16_13TeV.periodB.physics_Main.PhysCont.DAOD_SUSY2.grp16_v02_p2950
data16_13TeV.periodC.physics_Main.PhysCont.DAOD_SUSY2.grp16_v02_p2950
data16_13TeV.periodD.physics_Main.PhysCont.DAOD_SUSY2.grp16_v02_p2950
data16_13TeV.periodE.physics_Main.PhysCont.DAOD_SUSY2.grp16_v02_p2950
data16_13TeV.periodF.physics_Main.PhysCont.DAOD_SUSY2.grp16_v02_p2950
data16_13TeV.periodG.physics_Main.PhysCont.DAOD_SUSY2.grp16_v02_p2950
data16_13TeV.periodI.physics_Main.PhysCont.DAOD_SUSY2.grp16_v02_p2950
data16_13TeV.periodK.physics_Main.PhysCont.DAOD_SUSY2.grp16_v02_p2950
data16_13TeV.periodL.physics_Main.PhysCont.DAOD_SUSY2.grp16_v02_p2950

```

### 3.1.2 MC samples

#### 3.1.2.1 SM background

All MC samples are mc15c samples with offline release 20.7. All the background MC samples used in this analysis for each processes are shown the section A.1 in appendix. Each samples has its cross section, k-factor, generator efficiency and their equivalent integrated luminosity. Some samples may overlap with each other.

**t $\bar{t}$  and single top** The simulated events are generated by the POWHEG generator, and the CT10 PDF set is used. PYTHIA6 is also used for the parton shower model, with the PERUGIA 2012 tune. The mass of the top quark is assumed to be 172.5 GeV. The  $t\bar{t}$  samples are normalized to the next-to-next-to-leading order of cross section, while the single top samples are normalized to the next-to-leading order of cross section.

**W+jets and Z+jets** The simulated events are generated by the SHERPA v2.2.1. The matrix elements are calculated at the next-to-leading order for up to two partons, and at the leading order for up to four partons, by using the COMIX and OPENLOOPS generators. The samples are normalized to the next-to-next-to-leading order QCD cross section. The files are seperated according to the  $p_T$  of the vector boson and the presence of  $b$ -jet and  $c$ -jets.

**Diboson** The processes with four charged leptons ( $\ell\ell\ell\ell$ ), three charged leptons and one neutrino ( $\ell\ell\ell\nu$ ), and two charged leptons and two neutrinos ( $\ell\ell\nu\nu$ ) are

simulated by the SHERPA v2.2.1 generator. Diboson  $WW$ ,  $WZ$  and  $ZZ$  processes with four or six electroweak vertices are also used.

**Triboson** The triboson processes  $WWW$ ,  $WWZ$ ,  $WZZ$  and  $ZZZ$  with up to six charged leptons are simulated by the SHERPA v2.2.1 generator.

**tt+boson** The processes  $ttW$ ,  $ttZ$ ,  $ttWW$  and  $ttWZ$  are simulated by MADGRAPH v2.2.2 at the leading-order, with PYTHIA for the parton shower model.

**Higgs** The  $WH$  and  $ZH$  processes are generated by using PYTHIA 8 generator, and the A14 set of tuned parameters is used together with the NNPDF23LO PDF set. The  $ttH$  processes are generated by using MCATNLO generator, interfaced with HERWIGPP. The CT10 PDF tuning is used along with the CTEQ6L1-UE-EE-5 tuning of parton shower.

### 3.1.2.2 Signal

The signal MC samples simulate the signal process  $\tilde{\chi}_1^\pm \tilde{\chi}_2^0 \rightarrow W(\ell\nu)h$ . They are generated by the MADGRAPH v2.2.3, calculated at the leading-order matrix elements with up to two extra partons. PYTHIA version 8.186 and the A14 tune are also used for the modelling of the SUSY decay chain, parton showering and hadronisation. Parton luminosities are provided by the NNPDF23LO PDF set. Table A.12 shows the list of signal samples used in this analysis, with different hypothesized masses of  $\tilde{\chi}_1^\pm/\tilde{\chi}_2^0$  and  $\tilde{\chi}_1^0$ . These signal samples have been applied a selection that at least 2 leptons with  $p_T > 7$  GeV is required. The efficiencies due to this selection are applied and also shown in the table.

## 3.2 Pre-selection and event cleaning

The following pre-selections on the events are applied to reject background which did not come from the proton-proton collision and to ensure that the detector was working properly.

- **Good Run List** The events need to pass the good run list. (For data only)
- **LAr/Tile/SCT error** Events with data integrity errors in the SCT detector and the LAr and Tile calorimeter are removed. (For data only)

- **Primary Vertex** The events need to have a primary vertex, which is defined as the one with the largest  $\sum p_T^2$  of tracks, and has at least two tracks.
- **Cosmic Muon Veto** The events with cosmic muons need to be removed. The track of cosmic muon is identified by large impact parameters with respect to the primary vertex, with the condition that  $z_0^{PV} > 1$  mm or  $d_0^{PV} > 0.2$  mm.
- **Bad Muon Veto** The events with bad muons that does not come from the proton-proton collision need to be removed. The bad muon is identified by a large relative error in the ratio of electric charge to momentum ( $q/p$ ), with the condition that  $\sigma(q/p)/|q/p| > 0.2$ .
- **Bad Jet Veto** The events with bad jets that does not come from the proton-proton collision need to be removed. A jet with  $p_T < 20$  GeV or with the “LooseBad” quality by the Jet/Etmiss group is identified as a bad jet.

# **Chapter 4**

## **Pre-selection**

**4.1 Trigger selection**

**4.2 Event selection**

**4.3 Object definitions**

4.3.1 electrons and muons

4.3.2 jets

4.3.3 Missing transverse energy

## Chapter 5

# Signal Region

# Chapter 6

## Background estimation

The charge flip background and the fake lepton background are the two dominant backgrounds that their original particles in the final state come from the SM, but not the SUSY signal. Because of the mis-reconstruction, they pass the selections of the SRs. This type of background will be estimated by using the data-driven method.

### 6.1 charge flip background

#### 6.1.1 Sources for charge flip background

The charge flip background is due to the mis-identification of the sign of the charge of a lepton, after the reconstruction. The sign of the charge is determined by the direction of the curvature of the track. There are two main sources for the mis-identification for the direction of the curvature.

The first source is described by the figure 6.1. It is the case that the lepton interacts with the material of the detector, and a photon is emitted by the process of bremsstrahlung. The emitted photon further produces a pair of electron and positron, namely the  $\gamma$  conversion. As shown in figure 6.1, if the most of the energy is carried by the positron  $e^+$  (the purple track), the direction of the curvature of the reconstructed track (the orange track) will be reversed. Thus, the charge of the lepton is flipped. Because the amount of this mis-identification depends on the number of hits with the detector, and hence depends on  $|\eta|$  of the original track.

The second source is described by the figure 6.2. When the  $p_T$  of the lepton

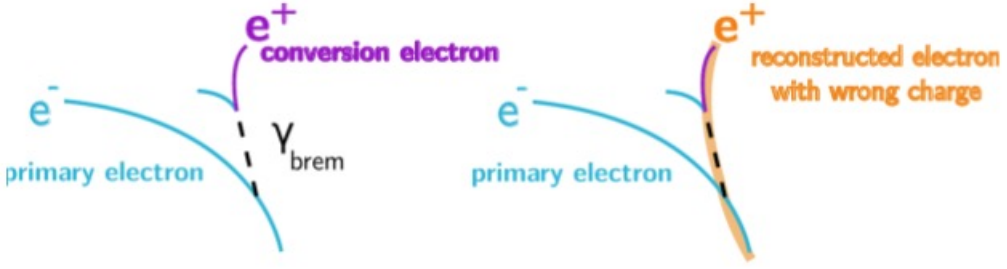


Figure 6.1: This shows how the track of the electron is incorrectly reconstructed (the orange track), due to the process of bremsstrahlung and  $\gamma$  conversion.

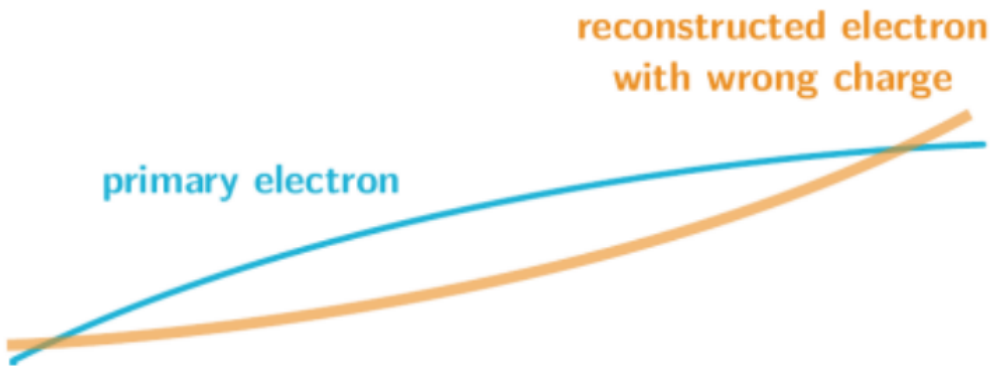


Figure 6.2: This shows how the track of the electron is incorrectly reconstructed (the orange track), due to very high  $p_T$  of the electron.

is very high, the track of the lepton will be almost a straight line. The curvature of the track will be close to zero, and the sign of the curvature will be difficult to distinguish. As a result, the sign of the charge of the lepton will be incorrectly assigned. The chance to have this problem obviously depends on  $p_T$  of the lepton.

Compared to an electron, the charge of a reconstructed muon will be less often to be mis-identified. The first reason is that a muon is heavier than an electron. This will reduce the chance of the process of bremsstrahlung. The second reason is that muons can reach to the muon spectrometer, which is the outer part of the detector, while most electrons cannot. This means that the length of the track of a muon, which can be detected by the tracker, is longer than that of an electron. Hence, the reconstructed curvature of the track for muons can be more accurate, and it reduces the chance of the mis-identification due to the high  $p_T$ . Because most of the charge flip background comes from electrons, we only estimate the

charge flip background for electrons.

### 6.1.2 Likelihood method

The probability that the charge of an electron is mis-identified is denoted by the charge-flip rate  $\epsilon_i$ , where the index  $i$  represents the dependency on the  $p_T$  and  $|\eta|$  of the electron. The value of index  $i$  is found by splitting the variables  $p_T$  and  $|\eta|$  into different 2-dimensional bins, and the binning for the  $p_T$  and  $|\eta|$  is described by the table 6.1. The index  $i$  of  $\epsilon_i$  is defined by the index of the bin.

Variable	Boundary of the bins
$p_T$ (GeV)	25, 60, 90, 130, 150, 1000
$ \eta $	0, 0.50, 1.00, 1.37, 1.52, 1.80, 2.00, 2.47

Table 6.1: Binning in  $p_T$  and  $|\eta|$  for the charge-flip rate  $\epsilon_i$ .

Suppose that, before the reconstruction, there are  $m_{OS}^{ij}$  opposite-sign events with the leading lepton in bin  $i$  and the subleading lepton in bin  $j$ , and similarly there are  $m_{SS}^{ij}$  same-sign events. After the reconstruction, due to the charge flip, there are  $M_{OS}^{ij}$  opposite-sign events and  $M_{SS}^{ij}$  same-sign events. The number of events after the reconstruction is given by

$$M_{OS}^{ij} = (1 - \epsilon_i)(1 - \epsilon_j)m_{OS}^{ij} + \epsilon_i(1 - \epsilon_j)m_{SS}^{ij} + (1 - \epsilon_i)\epsilon_j m_{SS}^{ij} + \epsilon_i\epsilon_j m_{OS}^{ij} \quad (6.1)$$

$$M_{SS}^{ij} = (1 - \epsilon_i)(1 - \epsilon_j)m_{SS}^{ij} + \epsilon_i(1 - \epsilon_j)m_{OS}^{ij} + (1 - \epsilon_i)\epsilon_j m_{OS}^{ij} + \epsilon_i\epsilon_j m_{SS}^{ij} \quad (6.2)$$

From equation 6.2, the number of reconstructed same-sign events due to the real opposite-sign events, i.e. the charge flip BG , denoted by  $N_{SS}^{ij}$ , is

$$N_{SS}^{ij} = \epsilon_i(1 - \epsilon_j)m_{OS}^{ij} + (1 - \epsilon_i)\epsilon_j m_{OS}^{ij} \quad (6.3)$$

In the SRs,  $m_{OS}^{ij}$  is the number of OS events before the reconstruction, but finally pass all selections in SRs.  $M_{OS}^{ij}$  is the total number of events that pass all selections in SRs, but replace SS requirement by OS. Because  $m_{OS}^{ij}$  is much larger than  $m_{SS}^{ij}$  and the measured charge-flip rate  $\epsilon_i$  is about  $10^{-3}$ ,  $m_{OS}^{ij}$  can be estimated by

$$M_{OS}^{ij} \approx (1 - \epsilon_i)(1 - \epsilon_j)m_{OS}^{ij} \quad (6.4)$$

$$m_{OS}^{ij} \approx \frac{M_{OS}^{ij}}{(1 - \epsilon_i)(1 - \epsilon_j)} \quad (6.5)$$

$$m_{OS}^{ij} \approx M_{OS}^{ij} \quad (6.6)$$

$$m_{OS}^{ij} \approx M_{OS}^{ij} + M_{SS}^{ij} \quad (6.7)$$

By substituting equation 6.7 into 6.3, the charge flip BG can be estimated by  $M_{OS}^{ij}$ ,  $M_{SS}^{ij}$  and the charge-flip rate  $\epsilon_i$ ,

$$N_{SS}^{ij} = \epsilon_i(1 - \epsilon_j)m_{OS}^{ij} + (1 - \epsilon_i)\epsilon_jm_{OS}^{ij} \quad (6.8)$$

$$= [\epsilon_i(1 - \epsilon_j) + (1 - \epsilon_i)\epsilon_j]m_{OS}^{ij} \quad (6.9)$$

$$\approx p_{ij}(M_{OS}^{ij} + M_{SS}^{ij}) \quad (6.10)$$

$$= p_{ij}N^{ij} \quad (6.11)$$

where  $p_{ij}$  and  $N^{ij}$  are

$$\begin{aligned} p_{ij} &= \epsilon_i(1 - \epsilon_j) + (1 - \epsilon_i)\epsilon_j \\ N^{ij} &= M_{OS}^{ij} + M_{SS}^{ij} \end{aligned} \quad (6.12)$$

The probability density function of  $N_{SS}^{ij}$ , with the given values of  $N^{ij}$  and  $\epsilon_i$ , can be described by the Poisson distribution with the mean value  $\lambda = p_{ij}N^{ij}$ .

$$P(N_{SS}^{ij}|N^{ij}, \epsilon_i, \epsilon_j) = \frac{\lambda^{N_{SS}^{ij}}e^{-\lambda}}{N_{SS}^{ij}!} \quad (6.13)$$

$$= \frac{(p_{ij}N^{ij})^{N_{SS}^{ij}}e^{-p_{ij}N^{ij}}}{N_{SS}^{ij}!} \quad (6.14)$$

In order to estimate the charge flip BG, we need to measure the charge-flip rate  $\epsilon_i$ . The charge-flip rate is measured as a function of  $p_T$  and  $|\eta|$  by using a likelihood method, based on the 2015 and 2016 data. A control region is used to select  $Z \rightarrow ee$  processes. Inside the control region, exactly 2 signal electrons are required. Also, a Z mass window of  $80 \text{ GeV} < m_{ll} < 100 \text{ GeV}$  is used. In this control region, the total number of events  $N^{ij}$  and the SS events  $N_{SS}^{ij}$  in each bin can be measured. By using the equation 6.14, the charge-flip rate  $\epsilon_i$  can be measured by using the following likelihood method.

The likelihood function  $L$  is defined by

$$L(\epsilon_i, \epsilon_j|N^{ij}, N_{SS}^{ij}) = \prod_{ij} P(N_{SS}^{ij}|N^{ij}, \epsilon_i, \epsilon_j) \quad (6.15)$$

$$= \prod_{ij} \frac{(p_{ij}N^{ij})^{N_{SS}^{ij}}e^{-p_{ij}N^{ij}}}{N_{SS}^{ij}!} \quad (6.16)$$

$$(6.17)$$

Given the measured values of  $N^{ij}$  and  $N_{SS}^{ij}$  in each bin, by maximizing the likelihood function over all possible values of  $\epsilon_i$ , the value of  $\epsilon_i$  can be estimated. By

taking the negative logarithm, it is equivalent to minimize  $-\ln L$ .

$$-\ln L = -\ln \prod_{ij} \frac{(p_{ij} N_{SS}^{ij})^{N_{SS}^{ij}} e^{-p_{ij} N_{SS}^{ij}}}{N_{SS}^{ij}!} \quad (6.18)$$

$$= -\sum_{ij} \ln \frac{(p_{ij} N_{SS}^{ij})^{N_{SS}^{ij}} e^{-p_{ij} N_{SS}^{ij}}}{N_{SS}^{ij}!} \quad (6.19)$$

$$= -\sum_{ij} \left[ N_{SS}^{ij} \ln(p_{ij} N_{SS}^{ij}) - p_{ij} N_{SS}^{ij} - \ln(N_{SS}^{ij}!) \right] \quad (6.20)$$

$$= -\sum_{ij} \left[ N_{SS}^{ij} \ln(p_{ij} N_{SS}^{ij}) - p_{ij} N_{SS}^{ij} \right] + \text{constant} \quad (6.21)$$

$$= -\sum_{ij} \left[ N_{SS}^{ij} \ln(N^{ij}[\epsilon_i(1-\epsilon_j) + (1-\epsilon_i)\epsilon_j]) - N^{ij}[\epsilon_i(1-\epsilon_j) + (1-\epsilon_i)\epsilon_j] \right] + \text{constant} \quad (6.22)$$

### 6.1.3 Background subtraction

By minimizing  $-\ln L$  described in the previous section, the value of the charge-flip rate  $\epsilon_i$  can be measured by using the data in the control region. In order to have better input values of  $N^{ij}$  and  $N_{SS}^{ij}$ , the number of events should mainly come from  $Z \rightarrow ee$  processes, and other processes should be subtracted. The number of events from other processes can be estimated by the sideband region:  $60 \text{ GeV} < m_{ll} < 80 \text{ GeV}$  and  $100 \text{ GeV} < m_{ll} < 120 \text{ GeV}$ . The corrected values of  $N^{ij}$  and  $N_{SS}^{ij}$  are given by

$$N_{80,100;\text{corrected}} = N_{80,100} - 20 \left( \frac{N_{60,80} + N_{80,100}}{20 + 20} \right) \quad (6.23)$$

In the sideband subtraction, the number of events in the sideband region should be normalized to the width of the central region. In general, given the number of events in the central region  $N_{\text{central}}$ , the left sideband region  $N_{\text{left}}$  and the right sideband region  $N_{\text{right}}$ , and their corresponding width  $w_{\text{central}}$ ,  $w_{\text{left}}$  and  $w_{\text{right}}$ , the corrected values  $N_{\text{central},\text{corrected}}$  are given by

$$N_{\text{central},\text{corrected}} = N_{\text{central}} - w_{\text{central}} \left( \frac{N_{\text{left}} + N_{\text{right}}}{w_{\text{left}} + w_{\text{right}}} \right) \quad (6.24)$$

### 6.1.4 Results without systematic uncertainty

Figure 6.3 shows the measured values of the charge-flip rate  $\epsilon_i$  by using the data. The errors only include the uncertainties in the likelihood method due to the statistics, denoted by  $\epsilon_{\text{lik,data}}$ .

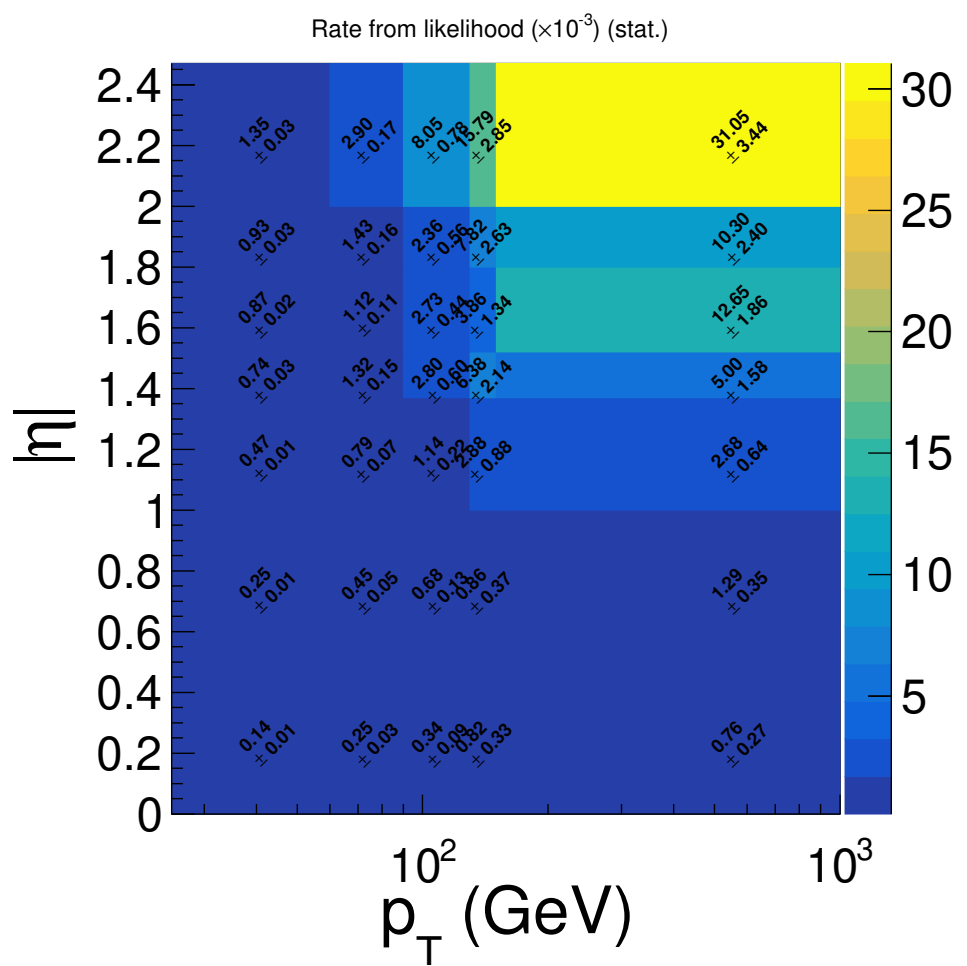


Figure 6.3: The measured values of the charge-flip rate  $\epsilon_i$  in data. Only uncertainties due to the likelihood method are included.

### 6.1.5 Systematic uncertainties due to background subtraction

The systematic uncertainties due to background subtraction is estimated by the variations of different central widths and sideband widths. The following are the nominal central region and sideband region, and their 4 variations.

The nominal background subtraction:

- Central region: 80 - 100 GeV; Sideband width: 20 GeV

The 4 variations for background subtraction:

- Central region: 80 - 100 GeV; Sideband width: 15 GeV
- Central region: 80 - 100 GeV; Sideband width: 25 GeV
- Central region: 75 - 105 GeV; Sideband width: 20 GeV
- Central region: 80 - 100 GeV; no background subtraction

For each bin, the largest deviation from the nominal among these variations is the systematic uncertainty due to background subtraction.

$$\sigma_{\text{bgk}} = \max\{|\sigma_{\text{nominal}} - \sigma_{\text{variation}}|\} \quad (6.25)$$

Figure 6.4 shows the variations of the resulting charge flip rate, due to these 4 variations.

### 6.1.6 Systematic uncertainties due to likelihood method

The systematic uncertainties due to likelihood method are estimated by the difference between the likelihood method and the MC truth method. In the MC truth method, the charge-flip rate is estimated by using the truth information in  $Z \rightarrow ee$  MC samples inside the control region. The control region requires exactly 2 signal electrons. The following are the procedures to match the reconstructed electron to the original electron, and hence the original electric charge can be found. Figure 6.5 shows how the original electron is found in the decay process described in figure 6.1. In this procedure, some reconstructed electrons will be ignored.

1. The reconstructed electron will be matched to the truth particle with the smallest  $\Delta R$  within the cone  $\Delta R < 0.1$ . If no any truth particles can be found inside the cone, the reconstructed electron will be ignored.

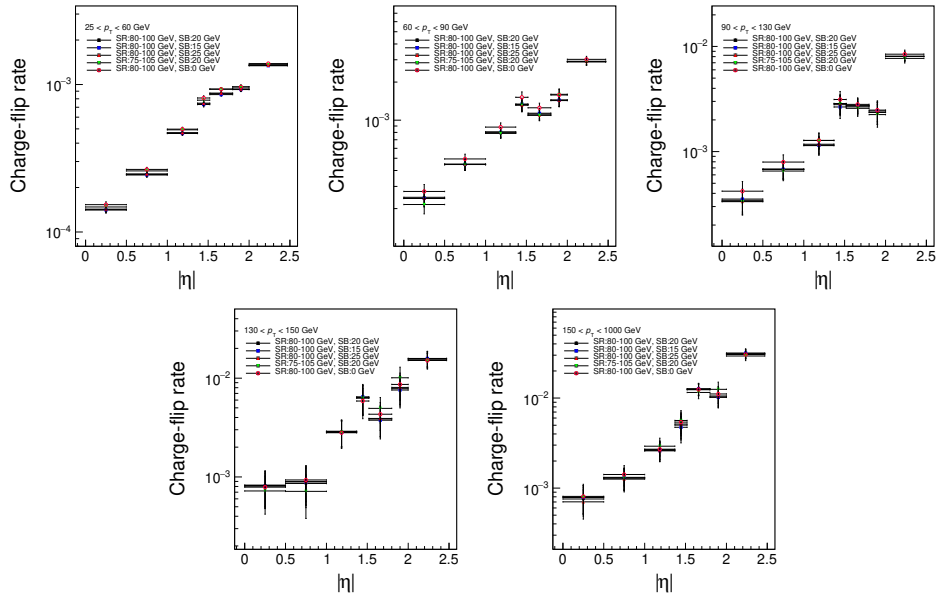


Figure 6.4: The systematic variations of the charge-flip rate  $\epsilon_i$  in data, due to the background subtraction.

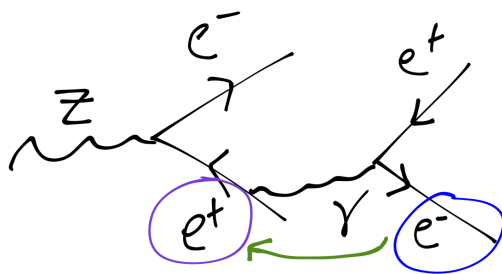


Figure 6.5: This diagram shows how the original electron is found through the decay chain.

2. If the truth particle is not an electron, it will be ignored.
3. If the origin of the truth electron is not a Z boson, it will be ignored.
4. If the daughter particle of the Z boson is not an electron, it will be ignored.
5. The charge of the daughter electron from the Z boson is the original charge of the reconstructed electron.

Only the events with two reconstructed electrons that are not ignored in the above procedure are considered.  $N_{\text{total}}$  is the total number of electrons in these events, and  $N_{\text{flipped}}$  is the number of electrons that the original charge and the reconstructed charge are different. By calculating the ratio in each bin, the charge flip rate can be estimated by using the MC truth information.

$$\epsilon_{\text{MC truth}} = \frac{N_{\text{flipped}}}{N_{\text{total}}} \quad (6.26)$$

The systematic uncertainties due to likelihood method  $\sigma_{\text{truth}}$  is then given by for MC,

$$\sigma_{\text{truth,MC}} = |\epsilon_{\text{lik,MC}} - \epsilon_{\text{MC truth}}| \quad (6.27)$$

for data,

$$\sigma_{\text{truth,data}} = \epsilon_{\text{lik,data}} \times \frac{\sigma_{\text{truth,MC}}}{\epsilon_{\text{lik,MC}}} \quad (6.28)$$

Figure 6.6 shows the comparison of the resulting charge flip rate, between the likelihood method and the MC truth method, by using the  $Z \rightarrow ee$  MC samples.

### 6.1.7 Results with total uncertainties

The total systematic uncertainties is the quadratic sum of systematic uncertainties due to the background subtraction and the likelihood method, described in section 6.1.5 and 6.1.6 respectively.

$$\sigma_{\text{sys}} = \sqrt{\sigma_{\text{bgk}}^2 + \sigma_{\text{truth}}^2} \quad (6.29)$$

The total uncertainties is the quadratic sum of the total systematic uncertainties and the statistical uncertainties in the likelihood method.

$$\sigma_{\text{tot}} = \sqrt{\sigma_{\text{sys}}^2 + \sigma_{\text{lik}}^2} \quad (6.30)$$

Figure 6.7 shows the measured values of the charge-flip rate  $\epsilon_i$  by using the data, with total uncertainties described in equation 6.30.

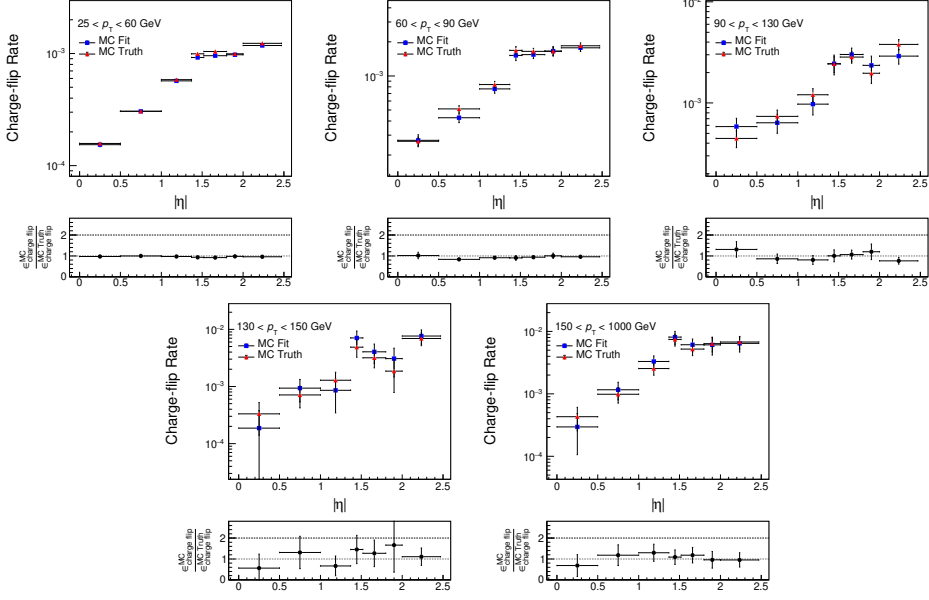


Figure 6.6: The comparison between the likelihood method and the MC truth method, by using the  $Z \rightarrow ee$  MC samples. Hence, the systematic uncertainties due to likelihood method can be estimated.

### 6.1.8 MC validation

The charge flip rate can be validated by using the  $Z \rightarrow ee$  MC samples. By using the equation 6.5 and 6.9,  $N_{SS}^{ij}$  can be approximated by

$$N_{SS}^{ij} = [\epsilon_i(1 - \epsilon_j) + (1 - \epsilon_i)\epsilon_j]m_{OS}^{ij} \quad (6.31)$$

$$\approx [\epsilon_i(1 - \epsilon_j) + (1 - \epsilon_i)\epsilon_j] \frac{M_{OS}^{ij}}{(1 - \epsilon_i)(1 - \epsilon_j)} \quad (6.32)$$

$$= \frac{\epsilon_i(1 - \epsilon_j) + (1 - \epsilon_i)\epsilon_j}{(1 - \epsilon_i)(1 - \epsilon_j)} M_{OS}^{ij} \quad (6.33)$$

Also, in the equation 6.2,  $m_{SS}^{ij}$  is zero for the  $Z \rightarrow ee$  MC samples, we have

$$M_{SS}^{ij} = \epsilon_i(1 - \epsilon_j)m_{OS}^{ij} + (1 - \epsilon_i)\epsilon_j m_{OS}^{ij} \quad (6.34)$$

$$= N_{SS}^{ij} \quad (6.35)$$

Hence, it is expected that

$$M_{SS}^{ij} \approx \frac{\epsilon_i(1 - \epsilon_j) + (1 - \epsilon_i)\epsilon_j}{(1 - \epsilon_i)(1 - \epsilon_j)} M_{OS}^{ij} \quad (6.36)$$

By weighting the OS events in MC with the weight,

$$\text{weight} = \frac{\epsilon_i(1 - \epsilon_j) + (1 - \epsilon_i)\epsilon_j}{(1 - \epsilon_i)(1 - \epsilon_j)} \quad (6.37)$$

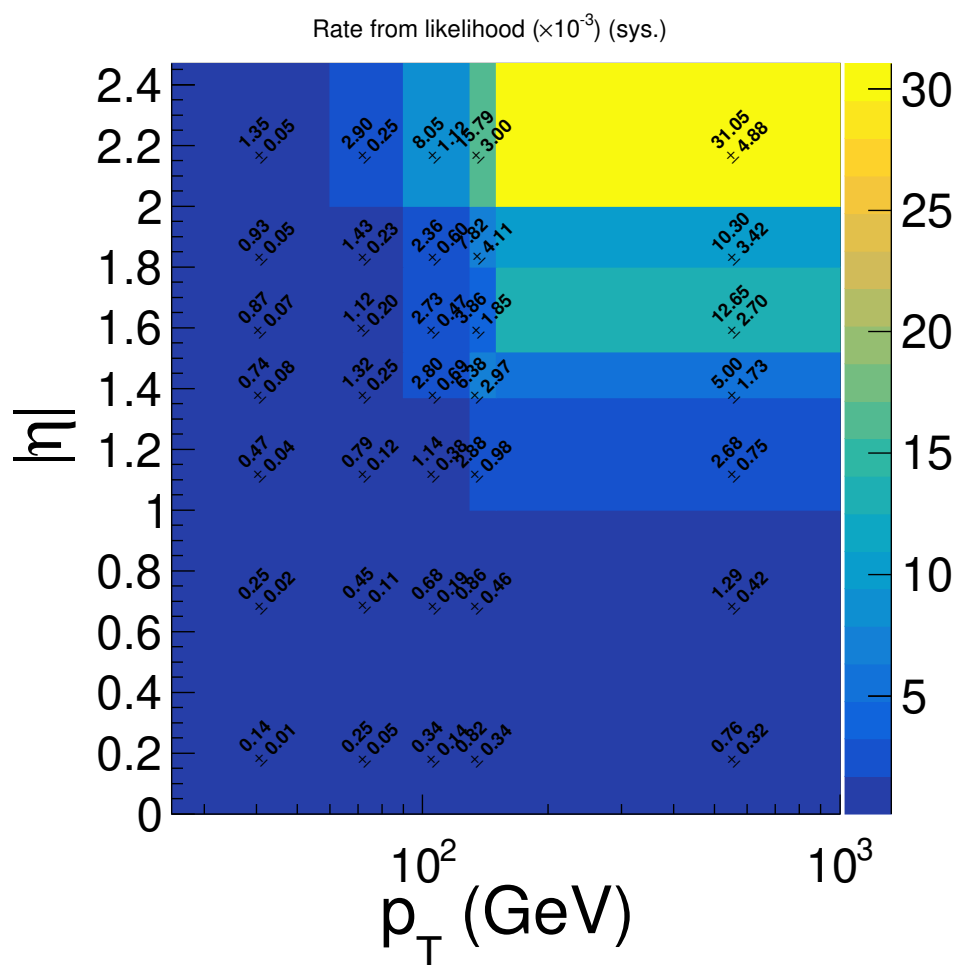


Figure 6.7: The measured values of the charge-flip rate  $\epsilon_i$  in data, with total uncertainties.

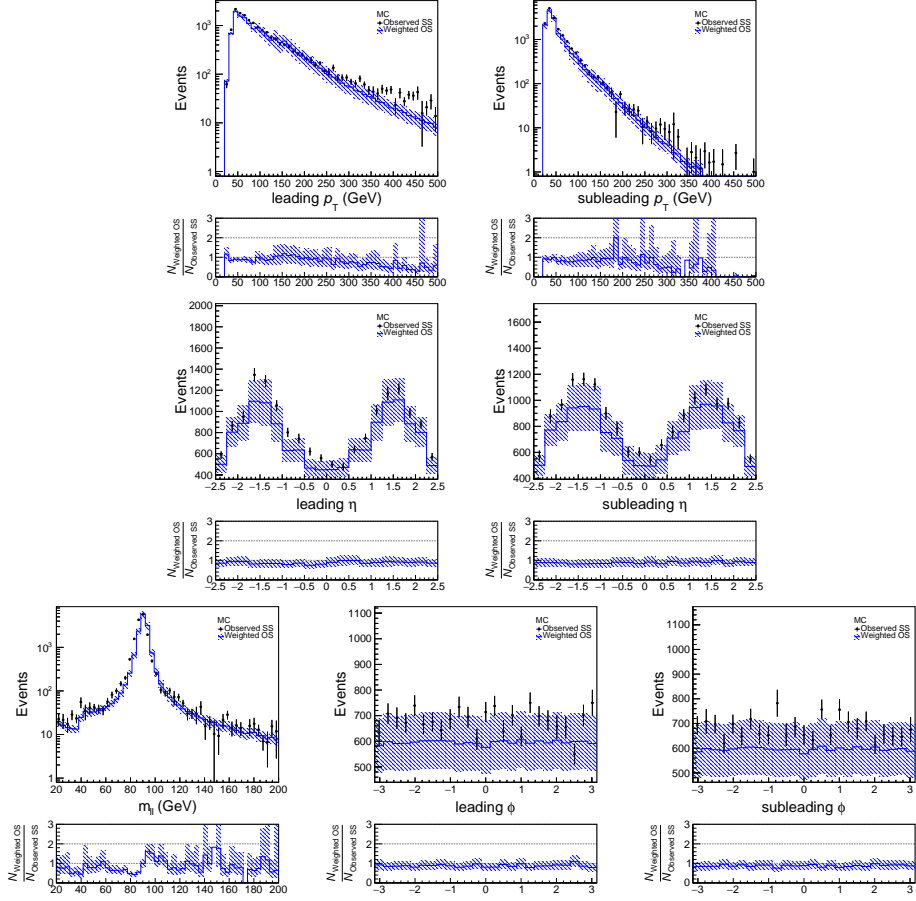


Figure 6.8: The comparison between the weighted OS events and the SS events, with different variables.

the weighted OS events and the SS events will be close to each other. This can be used to validate the charge flip rate. Figure shows the comparison between the weighted OS events and the SS events, with different variables. All event weights are applied, except the charge flip scale factor. The weighted OS events and the SS events agree within the uncertainties.

## 6.2 fake lepton background

### 6.2.1 Sources for fake lepton background

The fake lepton background is ascribed to the case that other particle like meson, hadron and photon is mis-identified as a lepton, after the reconstruction. Three types of fake lepton background are described as follows.

- Heavy-flavor fakes:

- It comes from semi-leptonic decays of heavy-quark (b or c) hadrons in jets
- Light-flavor fakes:
  - It comes from semi-leptonic decays of light-quark hadrons in jets
  - or is due to mis-reconstructions of jets with light-quark hadrons
- photon conversion:
  - It comes from the pair production from a photon

These leptons do not often pass the lepton identification cuts and have large impact parameters. They are also not well-isolated.

### 6.2.2 Matrix method

The fake lepton background is estimated by the matrix method. The input of this method is the real and fake efficiencies of electron and muon, in different bins of  $p_T$  and  $|\eta|$ , which is measured in the following sections. This method will estimate the amount of fake lepton background, by counting the number of loose and tight in data. The tight leptons in our analysis is the signal leptons, and the loose leptons is baseline leptons but not signal leptons.

The probability that a real electron (or muon) passes the signal selection (i.e. tight lepton) is denoted by the real efficiency  $\epsilon$ . The probability that a real electron (or muon) does not pass the signal selection (i.e. loose lepton) is denoted by  $\bar{\epsilon} = 1 - \epsilon$ . Similarly, the probability that a fake electron (or muon) passes the signal selection (i.e. tight lepton) is denoted by the fake efficiency  $f$ . The probability that a fake electron (or muon) does not pass the signal selection (i.e. loose lepton) is denoted by  $\bar{f} = 1 - f$ . Although there are no any subscripts and superscripts for the efficiencies  $\epsilon$  and  $f$ , these efficiencies are different for different flavours of the leptons (electron or muon), and also in different  $p_T$ - $|\eta|$  bins.

For simplicity, we first consider the case with only one leptons. We will then generalize to the case with two leptons. By the definition of the efficiencies, the relation between the number of real/fake leptons and the number of tight/loose leptons is given by the following matrix.

$$\begin{pmatrix} N_T \\ N_L \end{pmatrix} = \begin{pmatrix} \epsilon & f \\ \bar{\epsilon} & \bar{f} \end{pmatrix} \begin{pmatrix} N_R \\ N_F \end{pmatrix} \quad (6.38)$$

Because the number of tight/loose leptons can be counted in data,  $\begin{pmatrix} N_T \\ N_L \end{pmatrix}$  is known. By inverting the matrix, the original number of fake leptons can be calculated.

$$\begin{pmatrix} 0 \\ N_F \end{pmatrix} = \begin{pmatrix} 0 & 0 \\ 0 & 1 \end{pmatrix} \begin{pmatrix} N_R \\ N_F \end{pmatrix} \quad (6.39)$$

$$= \begin{pmatrix} 0 & 0 \\ 0 & 1 \end{pmatrix} \begin{pmatrix} \epsilon & f \\ \bar{\epsilon} & \bar{f} \end{pmatrix}^{-1} \begin{pmatrix} N_T \\ N_L \end{pmatrix}$$

The fake lepton background, which is the number of tight lepton due to the fake lepton,  $N'_T$ , can then be found, by re-apply the matrix in equation 6.38.

$$\begin{pmatrix} N'_T \\ N'_L \end{pmatrix} = \begin{pmatrix} \epsilon & f \\ \bar{\epsilon} & \bar{f} \end{pmatrix} \begin{pmatrix} 0 \\ N_F \end{pmatrix} \quad (6.40)$$

$$= \begin{pmatrix} \epsilon & f \\ \bar{\epsilon} & \bar{f} \end{pmatrix} \begin{pmatrix} 0 & 0 \\ 0 & 1 \end{pmatrix} \begin{pmatrix} \epsilon & f \\ \bar{\epsilon} & \bar{f} \end{pmatrix}^{-1} \begin{pmatrix} N_T \\ N_L \end{pmatrix}$$

$$N'_T = \begin{pmatrix} \epsilon & f \end{pmatrix} \begin{pmatrix} 0 & 0 \\ 0 & 1 \end{pmatrix} \begin{pmatrix} \epsilon & f \\ \bar{\epsilon} & \bar{f} \end{pmatrix}^{-1} \begin{pmatrix} N_T \\ N_L \end{pmatrix}$$

To generalize to the case with two leptons, equation 6.38 become

$$\begin{pmatrix} N_{TT} \\ N_{TL} \\ N_{LT} \\ N_{LL} \end{pmatrix} = \begin{pmatrix} \epsilon_1 \epsilon_2 & \epsilon_1 f_2 & f_1 \epsilon_2 & f_1 f_2 \\ \epsilon_1 \bar{\epsilon}_2 & \epsilon_1 \bar{f}_2 & f_1 \bar{\epsilon}_2 & f_1 \bar{f}_2 \\ \bar{\epsilon}_1 \epsilon_2 & \bar{\epsilon}_1 f_2 & \bar{f}_1 \epsilon_2 & \bar{f}_1 f_2 \\ \bar{\epsilon}_1 \bar{\epsilon}_2 & \bar{\epsilon}_1 \bar{f}_2 & \bar{f}_1 \bar{\epsilon}_2 & \bar{f}_1 \bar{f}_2 \end{pmatrix} \begin{pmatrix} N_{RR} \\ N_{RF} \\ N_{FR} \\ N_{FF} \end{pmatrix} \quad (6.41)$$

where the subscript 1 and 2 of the efficiencies denote the leading lepton and subleading lepton respectively. The two letters in the subscript of  $N$  describe the types of the leading and subleading lepton respectively.  $N_{RF}$ ,  $N_{FR}$ ,  $N_{FF}$  can be

found by inverting the matrix.

$$\begin{aligned}
\begin{pmatrix} 0 \\ N_{RF} \\ N_{FR} \\ N_{FF} \end{pmatrix} &= \begin{pmatrix} 0 & 0 & 0 & 0 \\ 0 & 1 & 0 & 0 \\ 0 & 0 & 1 & 0 \\ 0 & 0 & 0 & 1 \end{pmatrix} \begin{pmatrix} N_{RR} \\ N_{RF} \\ N_{FR} \\ N_{FF} \end{pmatrix} \\
&= \begin{pmatrix} 0 & 0 & 0 & 0 \\ 0 & 1 & 0 & 0 \\ 0 & 0 & 1 & 0 \\ 0 & 0 & 0 & 1 \end{pmatrix} \begin{pmatrix} \epsilon_1\epsilon_2 & \epsilon_1f_2 & f_1\epsilon_2 & f_1f_2 \\ \epsilon_1\bar{\epsilon}_2 & \epsilon_1\bar{f}_2 & f_1\bar{\epsilon}_2 & f_1\bar{f}_2 \\ \bar{\epsilon}_1\epsilon_2 & \bar{\epsilon}_1f_2 & \bar{f}_1\epsilon_2 & \bar{f}_1f_2 \\ \bar{\epsilon}_1\bar{\epsilon}_2 & \bar{\epsilon}_1\bar{f}_2 & \bar{f}_1\bar{\epsilon}_2 & \bar{f}_1\bar{f}_2 \end{pmatrix}^{-1} \begin{pmatrix} N_{TT} \\ N_{TL} \\ N_{LT} \\ N_{LL} \end{pmatrix}
\end{aligned} \tag{6.42}$$

The fake lepton background, which is the number of tight-tight lepton due to the fake lepton,  $N'_{TT}$ , can then be found.

$$\begin{aligned}
\begin{pmatrix} N'_{TT} \\ N'_{TL} \\ N'_{LT} \\ N'_{LL} \end{pmatrix} &= \begin{pmatrix} \epsilon_1\epsilon_2 & \epsilon_1f_2 & f_1\epsilon_2 & f_1f_2 \\ \epsilon_1\bar{\epsilon}_2 & \epsilon_1\bar{f}_2 & f_1\bar{\epsilon}_2 & f_1\bar{f}_2 \\ \bar{\epsilon}_1\epsilon_2 & \bar{\epsilon}_1f_2 & \bar{f}_1\epsilon_2 & \bar{f}_1f_2 \\ \bar{\epsilon}_1\bar{\epsilon}_2 & \bar{\epsilon}_1\bar{f}_2 & \bar{f}_1\bar{\epsilon}_2 & \bar{f}_1\bar{f}_2 \end{pmatrix} \begin{pmatrix} 0 \\ N_{RF} \\ N_{FR} \\ N_{FF} \end{pmatrix} \\
&= \begin{pmatrix} \epsilon_1\epsilon_2 & \epsilon_1f_2 & f_1\epsilon_2 & f_1f_2 \\ \epsilon_1\bar{\epsilon}_2 & \epsilon_1\bar{f}_2 & f_1\bar{\epsilon}_2 & f_1\bar{f}_2 \\ \bar{\epsilon}_1\epsilon_2 & \bar{\epsilon}_1f_2 & \bar{f}_1\epsilon_2 & \bar{f}_1f_2 \\ \bar{\epsilon}_1\bar{\epsilon}_2 & \bar{\epsilon}_1\bar{f}_2 & \bar{f}_1\bar{\epsilon}_2 & \bar{f}_1\bar{f}_2 \end{pmatrix} \begin{pmatrix} 0 & 0 & 0 & 0 \\ 0 & 1 & 0 & 0 \\ 0 & 0 & 1 & 0 \\ 0 & 0 & 0 & 1 \end{pmatrix} \begin{pmatrix} \epsilon_1\epsilon_2 & \epsilon_1f_2 & f_1\epsilon_2 & f_1f_2 \\ \epsilon_1\bar{\epsilon}_2 & \epsilon_1\bar{f}_2 & f_1\bar{\epsilon}_2 & f_1\bar{f}_2 \\ \bar{\epsilon}_1\epsilon_2 & \bar{\epsilon}_1f_2 & \bar{f}_1\epsilon_2 & \bar{f}_1f_2 \\ \bar{\epsilon}_1\bar{\epsilon}_2 & \bar{\epsilon}_1\bar{f}_2 & \bar{f}_1\bar{\epsilon}_2 & \bar{f}_1\bar{f}_2 \end{pmatrix}^{-1} \begin{pmatrix} N_{TT} \\ N_{TL} \\ N_{LT} \\ N_{LL} \end{pmatrix} \\
N'_{TT} &= \left( \begin{matrix} \epsilon_1\epsilon_2 & \epsilon_1f_2 & f_1\epsilon_2 & f_1f_2 \end{matrix} \right) \begin{pmatrix} 0 & 0 & 0 & 0 \\ 0 & 1 & 0 & 0 \\ 0 & 0 & 1 & 0 \\ 0 & 0 & 0 & 1 \end{pmatrix} \begin{pmatrix} \epsilon_1\epsilon_2 & \epsilon_1f_2 & f_1\epsilon_2 & f_1f_2 \\ \epsilon_1\bar{\epsilon}_2 & \epsilon_1\bar{f}_2 & f_1\bar{\epsilon}_2 & f_1\bar{f}_2 \\ \bar{\epsilon}_1\epsilon_2 & \bar{\epsilon}_1f_2 & \bar{f}_1\epsilon_2 & \bar{f}_1f_2 \\ \bar{\epsilon}_1\bar{\epsilon}_2 & \bar{\epsilon}_1\bar{f}_2 & \bar{f}_1\bar{\epsilon}_2 & \bar{f}_1\bar{f}_2 \end{pmatrix}^{-1} \begin{pmatrix} N_{TT} \\ N_{TL} \\ N_{LT} \\ N_{LL} \end{pmatrix}
\end{aligned} \tag{6.43}$$

Equation 6.43 can be applied to any combination of the flavour,  $p_T$  and  $|\eta|$  of the leading and subleading lepton. In principle, the total amount of fake lepton background should be the summation of all combination of the flavour,  $p_T$  and  $|\eta|$ . For a particular combination, the counting result of the tight/loose leptons in

data  $\begin{pmatrix} N_{TT} \\ N_{TL} \\ N_{LT} \\ N_{LL} \end{pmatrix}$  can be split into “one”, which is the contribution by one event.

$$\begin{pmatrix} N_{TT} \\ N_{TL} \\ N_{LT} \\ N_{LL} \end{pmatrix} = \sum_{i=1}^{N_{TT}} \begin{pmatrix} 1 \\ 0 \\ 0 \\ 0 \end{pmatrix} + \sum_{i=1}^{N_{TL}} \begin{pmatrix} 0 \\ 1 \\ 0 \\ 0 \end{pmatrix} + \sum_{i=1}^{N_{LT}} \begin{pmatrix} 0 \\ 0 \\ 1 \\ 0 \end{pmatrix} + \sum_{i=1}^{N_{LL}} \begin{pmatrix} 0 \\ 0 \\ 0 \\ 1 \end{pmatrix} \quad (6.44)$$

Because equation 6.43 is a linear function, we can first calculate the small contribution of  $N'_{TT}$  from one event, and assign this value as a weight to the event. This weight is called the fake weight of the event. The total fake lepton background is then the sum of the fake weight of all events in data. For example, if the pair of the two leptons is a tight-tight pair, the fake weight of this event is  $N'_{TT}$  in the following equation.

$$N'_{TT} = \begin{pmatrix} \epsilon_1\epsilon_2 & \epsilon_1f_2 & f_1\epsilon_2 & f_1f_2 \end{pmatrix} \begin{pmatrix} 0 & 0 & 0 & 0 \\ 0 & 1 & 0 & 0 \\ 0 & 0 & 1 & 0 \\ 0 & 0 & 0 & 1 \end{pmatrix} \begin{pmatrix} \epsilon_1\epsilon_2 & \epsilon_1f_2 & f_1\epsilon_2 & f_1f_2 \\ \epsilon_1\bar{\epsilon}_2 & \epsilon_1\bar{f}_2 & f_1\bar{\epsilon}_2 & f_1\bar{f}_2 \\ \bar{\epsilon}_1\epsilon_2 & \bar{\epsilon}_1f_2 & \bar{f}_1\epsilon_2 & \bar{f}_1f_2 \\ \bar{\epsilon}_1\bar{\epsilon}_2 & \bar{\epsilon}_1\bar{f}_2 & \bar{f}_1\bar{\epsilon}_2 & \bar{f}_1\bar{f}_2 \end{pmatrix}^{-1} \begin{pmatrix} 1 \\ 0 \\ 0 \\ 0 \end{pmatrix} \quad (6.45)$$

where the flavours,  $p_T$  and  $|\eta|$  of the efficiencies is simply the flavours,  $p_T$  and  $|\eta|$  of the leading and subleading lepton in this event.

By calculating the inverse of the matrix, equation 6.43 can be simplified. First, we define a variable  $d$ .

$$d = (\epsilon_1 - f_1)(\epsilon_2 - f_2) \quad (6.46)$$

The inverse of the matrix is given by

$$\begin{pmatrix} \epsilon_1\epsilon_2 & \epsilon_1f_2 & f_1\epsilon_2 & f_1f_2 \\ \epsilon_1\bar{\epsilon}_2 & \epsilon_1\bar{f}_2 & f_1\bar{\epsilon}_2 & f_1\bar{f}_2 \\ \bar{\epsilon}_1\epsilon_2 & \bar{\epsilon}_1f_2 & \bar{f}_1\epsilon_2 & \bar{f}_1f_2 \\ \bar{\epsilon}_1\bar{\epsilon}_2 & \bar{\epsilon}_1\bar{f}_2 & \bar{f}_1\bar{\epsilon}_2 & \bar{f}_1\bar{f}_2 \end{pmatrix}^{-1} = \frac{1}{d} \begin{pmatrix} \bar{f}_1\bar{f}_2 & -\bar{f}_1f_2 & -f_1\bar{f}_2 & f_1f_2 \\ -\bar{f}_1\bar{\epsilon}_2 & \bar{f}_1\epsilon_2 & f_1\bar{\epsilon}_2 & -f_1\epsilon_2 \\ -\bar{\epsilon}_1\bar{f}_2 & \bar{\epsilon}_1f_2 & \epsilon_1\bar{f}_2 & -\epsilon_1f_2 \\ \bar{\epsilon}_1\bar{\epsilon}_2 & -\bar{\epsilon}_1\epsilon_2 & -\epsilon_1\bar{\epsilon}_2 & \epsilon_1\epsilon_2 \end{pmatrix} \quad (6.47)$$

Equation 6.43 becomes

$$\begin{aligned}
N'_{TT} &= \left( \begin{array}{cccc} \epsilon_1 \epsilon_2 & \epsilon_1 f_2 & f_1 \epsilon_2 & f_1 f_2 \end{array} \right) \left( \begin{array}{cccc} 0 & 0 & 0 & 0 \\ 0 & 1 & 0 & 0 \\ 0 & 0 & 1 & 0 \\ 0 & 0 & 0 & 1 \end{array} \right) \frac{1}{d} \left( \begin{array}{cccc} \bar{f}_1 \bar{f}_2 & -\bar{f}_1 f_2 & -f_1 \bar{f}_2 & f_1 f_2 \\ -\bar{f}_1 \bar{\epsilon}_2 & \bar{f}_1 \epsilon_2 & f_1 \bar{\epsilon}_2 & -f_1 \epsilon_2 \\ -\bar{\epsilon}_1 \bar{f}_2 & \bar{\epsilon}_1 f_2 & \epsilon_1 \bar{f}_2 & -\epsilon_1 f_2 \\ \bar{\epsilon}_1 \bar{\epsilon}_2 & -\bar{\epsilon}_1 \epsilon_2 & -\epsilon_1 \bar{\epsilon}_2 & \epsilon_1 \epsilon_2 \end{array} \right) \left( \begin{array}{c} N_{TT} \\ N_{TL} \\ N_{LT} \\ N_{LL} \end{array} \right) \\
&= \frac{1}{d} \left( \begin{array}{cccc} \epsilon_1 \epsilon_2 & \epsilon_1 f_2 & f_1 \epsilon_2 & f_1 f_2 \end{array} \right) \left( \begin{array}{cccc} 0 & 0 & 0 & 0 \\ -\bar{f}_1 \bar{\epsilon}_2 & \bar{f}_1 \epsilon_2 & f_1 \bar{\epsilon}_2 & -f_1 \epsilon_2 \\ -\bar{\epsilon}_1 \bar{f}_2 & \bar{\epsilon}_1 f_2 & \epsilon_1 \bar{f}_2 & -\epsilon_1 f_2 \\ \bar{\epsilon}_1 \bar{\epsilon}_2 & -\bar{\epsilon}_1 \epsilon_2 & -\epsilon_1 \bar{\epsilon}_2 & \epsilon_1 \epsilon_2 \end{array} \right) \left( \begin{array}{c} N_{TT} \\ N_{TL} \\ N_{LT} \\ N_{LL} \end{array} \right)
\end{aligned} \tag{6.48}$$

For a tight-tight pair,

$$\text{fake weight} = \frac{1}{d}(-\epsilon_1 \bar{f}_1 \bar{\epsilon}_2 f_2 - \bar{\epsilon}_1 f_1 \epsilon_2 \bar{f}_2 + \bar{\epsilon}_1 f_1 \bar{\epsilon}_2 f_2) \tag{6.49}$$

For a tight-loose pair,

$$\begin{aligned}
\text{fake weight} &= \frac{1}{d}(\epsilon_1 \bar{f}_1 \epsilon_2 f_2 + \bar{\epsilon}_1 f_1 \epsilon_2 f_2 - \bar{\epsilon}_1 f_1 \epsilon_2 f_2) \\
&= \frac{\epsilon_1 \bar{f}_1 \epsilon_2 f_2}{d}
\end{aligned} \tag{6.50}$$

For a loose-tight pair,

$$\begin{aligned}
\text{fake weight} &= \frac{1}{d}(\epsilon_1 f_1 \bar{\epsilon}_2 f_2 + \epsilon_1 f_1 \epsilon_2 \bar{f}_2 - \epsilon_1 f_1 \bar{\epsilon}_2 f_2) \\
&= \frac{\epsilon_1 f_1 \epsilon_2 \bar{f}_2}{d}
\end{aligned} \tag{6.51}$$

For a loose-loose pair,

$$\begin{aligned}
\text{fake weight} &= \frac{1}{d}(-\epsilon_1 f_1 \epsilon_2 f_2 - \epsilon_1 f_1 \epsilon_2 f_2 + \epsilon_1 f_1 \epsilon_2 f_2) \\
&= -\frac{\epsilon_1 f_1 \epsilon_2 f_2}{d}
\end{aligned} \tag{6.52}$$

### 6.2.3 Measurement of real efficiencies

## **Chapter 7**

# **Validation regions**

# Appendix A

## List of MC samples

### A.1 List of background MC samples

Dataset ID	Process	Tags	Cross section [pb]	k-factor	Generator efficiency	$\mathcal{L}_{int} [\text{fb}^{-1}]$
364156	Sherpa_221_NNPDF30NNLO_Wmumu_MAXHTPTV0_70_CVetoBVeto	e5340_s2726_r7772_r7676_p2949	19143.0000	0.97	0.824	1.616
364157	Sherpa_221_NNPDF30NNLO_Wmumu_MAXHTPTV0_70_CFilterBVeto	e5340_s2726_r7772_r7676_p2949	19121.0000	0.97	0.130	4.071
364158	Sherpa_221_NNPDF30NNLO_Wmumu_MAXHTPTV0_70_BFilter	e5340_s2726_r7772_r7676_p2949	19135.0000	0.97	0.044	21.032
364159	Sherpa_221_NNPDF30NNLO_Wmumu_MAXHTPTV70_140_CVetoBVeto	e5340_s2726_r7772_r7676_p2949	944.8500	0.97	0.675	23.912
364160	Sherpa_221_NNPDF30NNLO_Wmumu_MAXHTPTV70_140_CFilterBVeto	e5340_s2726_r7772_r7676_p2949	937.7800	0.97	0.235	46.173
364161	Sherpa_221_NNPDF30NNLO_Wmumu_MAXHTPTV70_140_BFilter	e5340_s2726_r7772_r7676_p2949	944.6300	0.97	0.076	283.269
364162	Sherpa_221_NNPDF30NNLO_Wmumu_MAXHTPTV140_280_CVetoBVeto	e5340_s2726_r7772_r7676_p2949	339.5400	0.97	0.626	47.919
364163	Sherpa_221_NNPDF30NNLO_Wmumu_MAXHTPTV140_280_CFilterBVeto	e5340_s2726_r7772_r7676_p2949	340.0600	0.97	0.289	77.568
364164	Sherpa_221_NNPDF30NNLO_Wmumu_MAXHTPTV140_280_BFilter	e5340_s2726_r7772_r7676_p2949	339.5400	0.97	0.109	686.449
364165	Sherpa_221_NNPDF30NNLO_Wmumu_MAXHTPTV280_500_CVetoBVeto	e5340_s2726_r7772_r7676_p2949	72.0670	0.97	0.546	129.289
364166	Sherpa_221_NNPDF30NNLO_Wmumu_MAXHTPTV280_500_CFilterBVeto	e5340_s2726_r7772_r7676_p2949	72.1980	0.97	0.317	133.034
364167	Sherpa_221_NNPDF30NNLO_Wmumu_MAXHTPTV280_500_BFilter	e5340_s2726_r7772_r7676_p2949	72.0450	0.97	0.133	317.464
364168	Sherpa_221_NNPDF30NNLO_Wmumu_MAXHTPTV500_1000	e5340_s2726_r7772_r7676_p2949	15.0100	0.97	1.000	405.866
364169	Sherpa_221_NNPDF30NNLO_Wmumu_MAXHTPTV1000_E_CMS	e5340_s2726_r7772_r7676_p2949	1.2344	0.97	1.000	3305.737
364170	Sherpa_221_NNPDF30NNLO_Wenu_MAXHTPTV0_70_CVetoBVeto	e5340_s2726_r7772_r7676_p2949	19127.0000	0.97	0.824	1.617
364171	Sherpa_221_NNPDF30NNLO_Wenu_MAXHTPTV0_70_CFilterBVeto	e5340_s2726_r7772_r7676_p2949	19130.0000	0.97	0.130	4.074
364172	Sherpa_221_NNPDF30NNLO_Wenu_MAXHTPTV0_70_BFilter	e5340_s2726_r7772_r7676_p2949	19135.0000	0.97	0.044	20.272
364173	Sherpa_221_NNPDF30NNLO_Wenu_MAXHTPTV70_140_CVetoBVeto	e5340_s2726_r7772_r7676_p2949	942.5800	0.97	0.669	23.973
364174	Sherpa_221_NNPDF30NNLO_Wenu_MAXHTPTV70_140_CFilterBVeto	e5340_s2726_r7772_r7676_p2949	945.6700	0.97	0.228	46.963
364175	Sherpa_221_NNPDF30NNLO_Wenu_MAXHTPTV70_140_BFilter	e5340_s2726_r7772_r7676_p2949	945.1500	0.97	0.103	103.368
364176	Sherpa_221_NNPDF30NNLO_Wenu_MAXHTPTV140_280_CVetoBVeto	e5340_s2726_r7772_r7676_p2949	339.8100	0.97	0.597	50.200
364177	Sherpa_221_NNPDF30NNLO_Wenu_MAXHTPTV140_280_CFilterBVeto	e5340_s2726_r7772_r7676_p2949	339.8700	0.97	0.290	77.584
364178	Sherpa_221_NNPDF30NNLO_Wenu_MAXHTPTV140_280_BFilter	e5340_s2726_r7772_r7676_p2949	339.4800	0.97	0.109	687.518
364179	Sherpa_221_NNPDF30NNLO_Wenu_MAXHTPTV280_500_CVetoBVeto	e5340_s2726_r7772_r7676_p2949	72.0840	0.97	0.544	129.323
364180	Sherpa_221_NNPDF30NNLO_Wenu_MAXHTPTV280_500_CFilterBVeto	e5340_s2726_r7772_r7676_p2949	72.1280	0.97	0.317	133.693
364181	Sherpa_221_NNPDF30NNLO_Wenu_MAXHTPTV280_500_BFilter	e5340_s2726_r7772_r7676_p2949	72.1130	0.97	0.134	315.726
364182	Sherpa_221_NNPDF30NNLO_Wenu_MAXHTPTV500_1000	e5340_s2726_r7772_r7676_p2949	15.2240	0.97	1.000	400.587
364183	Sherpa_221_NNPDF30NNLO_Wenu_MAXHTPTV1000_E_CMS	e5340_s2726_r7772_r7676_p2949	1.2334	0.97	1.000	3298.389
364184	Sherpa_221_NNPDF30NNLO_Wtaunu_MAXHTPTV70_20_CVetoBVeto	e5340_s2726_r7772_r7676_p2949	19152.0000	0.97	0.825	1.617
364185	Sherpa_221_NNPDF30NNLO_Wtaunu_MAXHTPTV70_20_CFilterBVeto	e5340_s2726_r7772_r7676_p2949	19153.0000	0.97	0.129	4.105
364186	Sherpa_221_NNPDF30NNLO_Wtaunu_MAXHTPTV70_20_BFilter	e5340_s2726_r7772_r7676_p2949	19163.0000	0.97	0.045	20.834
364187	Sherpa_221_NNPDF30NNLO_Wtaunu_MAXHTPTV70_140_CVetoBVeto	e5340_s2726_r7772_r7676_p2949	947.6500	0.97	0.674	23.903
364188	Sherpa_221_NNPDF30NNLO_Wtaunu_MAXHTPTV70_140_CFilterBVeto	e5340_s2726_r7772_r7676_p2949	946.7300	0.97	0.222	48.307
364189	Sherpa_221_NNPDF30NNLO_Wtaunu_MAXHTPTV70_140_BFilter	e5340_s2726_r7772_r7676_p2949	943.3000	0.97	0.104	103.602
364190	Sherpa_221_NNPDF30NNLO_Wtaunu_MAXHTPTV140_280_CVetoBVeto	e5340_s2726_r7772_r7676_p2949	339.3600	0.97	0.596	50.427
364191	Sherpa_221_NNPDF30NNLO_Wtaunu_MAXHTPTV140_280_CFilterBVeto	e5340_s2726_r7772_r7676_p2949	339.6300	0.97	0.290	76.903
364192	Sherpa_221_NNPDF30NNLO_Wtaunu_MAXHTPTV140_280_BFilter	e5340_s2726_r7772_r7676_p2949	339.5400	0.97	0.118	632.798
364193	Sherpa_221_NNPDF30NNLO_Wtaunu_MAXHTPTV280_500_CVetoBVeto	e5340_s2726_r7772_r7676_p2949	72.0650	0.92	0.546	136.270
364194	Sherpa_221_NNPDF30NNLO_Wtaunu_MAXHTPTV280_500_CFilterBVeto	e5340_s2726_r7772_r7676_p2949	71.9760	0.97	0.316	133.773
364195	Sherpa_221_NNPDF30NNLO_Wtaunu_MAXHTPTV280_500_BFilter	e5340_s2726_r7772_r7676_p2949	72.0260	0.97	0.134	314.868
364196	Sherpa_221_NNPDF30NNLO_Wtaunu_MAXHTPTV500_1000	e5340_s2726_r7772_r7676_p2949	15.0460	0.97	1.000	407.258
364197	Sherpa_221_NNPDF30NNLO_Wtaunu_MAXHTPTV1000_E_CMS	e5340_s2726_r7772_r7676_p2949	1.2339	0.97	1.000	3296.218

Table A.1: List of simulated W+jets processes

Dataset ID	Process	Tags	Cross section [pb]	k-factor	Generator efficiency	$\mathcal{L}_{int}[\text{fb}^{-1}]$
364100	Sherpa_221_NNPDF30NNLO_Zmumu_MAXHTPTV0_70_CVetoBVeto	e5271_s2726_r7772_r7676_p2949	1983.0000	0.98	0.822	4.964
364101	Sherpa_221_NNPDF30NNLO_Zmumu_MAXHTPTV0_70_CFilterBVeto	e5271_s2726_r7772_r7676_p2949	1978.4000	0.98	0.113	22.540
364102	Sherpa_221_NNPDF30NNLO_Zmumu_MAXHTPTV0_70_BFilter	e5271_s2726_r7772_r7676_p2949	1982.2000	0.98	0.064	63.719
364103	Sherpa_221_NNPDF30NNLO_Zmumu_MAXHTPTV70_140_CVetoBVeto	e5271_s2726_r7772_r7676_p2949	108.9200	0.98	0.689	80.890
364104	Sherpa_221_NNPDF30NNLO_Zmumu_MAXHTPTV70_140_CFilterBVeto	e5271_s2726_r7772_r7676_p2949	109.4200	0.98	0.186	99.279
364105	Sherpa_221_NNPDF30NNLO_Zmumu_MAXHTPTV70_140_BFilter	e5271_s2726_r7772_r7676_p2949	108.9100	0.98	0.114	488.459
364106	Sherpa_221_NNPDF30NNLO_Zmumu_MAXHTPTV140_280_CVetoBVeto	e5271_s2726_r7772_r7676_p2949	39.8780	0.98	0.609	208.736
364107	Sherpa_221_NNPDF30NNLO_Zmumu_MAXHTPTV140_280_CFilterBVeto	e5271_s2726_r7772_r7676_p2949	39.7950	0.98	0.233	326.653
364108	Sherpa_221_NNPDF30NNLO_Zmumu_MAXHTPTV140_280_BFilter	e5271_s2726_r7772_r7676_p2949	39.9080	0.98	0.146	2169.169
364109	Sherpa_221_NNPDF30NNLO_Zmumu_MAXHTPTV280_500_CVetoBVeto	e5271_s2726_r7772_r7676_p2949	8.5375	0.98	0.559	423.925
364110	Sherpa_221_NNPDF30NNLO_Zmumu_MAXHTPTV280_500_CFilterBVeto	e5271_s2726_r7772_r7676_p2949	8.5403	0.98	0.265	446.324
364111	Sherpa_221_NNPDF30NNLO_Zmumu_MAXHTPTV280_500_BFilter	e5271_s2726_r7772_r7676_p2949	8.4932	0.98	0.176	1355.672
364112	Sherpa_221_NNPDF30NNLO_Zmumu_MAXHTPTV500_1000	e5271_s2726_r7772_r7676_p2949	1.7881	0.98	1.000	1697.947
364113	Sherpa_221_NNPDF30NNLO_Zmumu_MAXHTPTV1000_E_CMS	e5271_s2726_r7772_r7676_p2949	0.1477	0.98	1.000	6860.515
364114	Sherpa_221_NNPDF30NNLO_Zee_MAXHTPTV70_140_CVetoBVeto	e5299_s2726_r7772_r7676_p2949	1981.8000	0.98	0.821	4.979
364115	Sherpa_221_NNPDF30NNLO_Zee_MAXHTPTV70_140_CFilterBVeto	e5299_s2726_r7772_r7676_p2949	1980.8000	0.98	0.113	22.646
364116	Sherpa_221_NNPDF30NNLO_Zee_MAXHTPTV70_BFilter	e5299_s2726_r7772_r7676_p2949	1981.7000	0.98	0.064	63.937
364117	Sherpa_221_NNPDF30NNLO_Zee_MAXHTPTV70_140_CVetoBVeto	e5299_s2726_r7772_r7676_p2949	110.5000	0.98	0.690	79.645
364118	Sherpa_221_NNPDF30NNLO_Zee_MAXHTPTV70_140_CFilterBVeto	e5299_s2726_r7772_r7676_p2949	110.6300	0.98	0.184	99.477
364119	Sherpa_221_NNPDF30NNLO_Zee_MAXHTPTV70_140_BFilter	e5299_s2726_r7772_r7676_p2949	110.3100	0.98	0.114	475.689
364120	Sherpa_221_NNPDF30NNLO_Zee_MAXHTPTV140_280_CVetoBVeto	e5299_s2726_r7772_r7676_p2949	40.7310	0.98	0.615	202.772
364121	Sherpa_221_NNPDF30NNLO_Zee_MAXHTPTV140_280_CFilterBVeto	e5299_s2726_r7772_r7676_p2949	40.6700	0.98	0.230	324.184
364122	Sherpa_221_NNPDF30NNLO_Zee_MAXHTPTV140_280_BFilter	e5299_s2726_r7772_r7676_p2949	40.6430	0.98	0.150	2078.998
364123	Sherpa_221_NNPDF30NNLO_Zee_MAXHTPTV280_500_CVetoBVeto	e5299_s2726_r7772_r7676_p2949	8.6743	0.98	0.561	407.078
364124	Sherpa_221_NNPDF30NNLO_Zee_MAXHTPTV280_500_CFilterBVeto	e5299_s2726_r7772_r7676_p2949	8.6711	0.98	0.263	444.808
364125	Sherpa_221_NNPDF30NNLO_Zee_MAXHTPTV280_500_BFilter	e5299_s2726_r7772_r7676_p2949	8.6766	0.98	0.172	1356.645
364126	Sherpa_221_NNPDF30NNLO_Zee_MAXHTPTV500_1000	e5299_s2726_r7772_r7676_p2949	1.8081	0.98	1.000	1686.255
364127	Sherpa_221_NNPDF30NNLO_Zee_MAXHTPTV1000_E_CMS	e5299_s2726_r7772_r7676_p2949	0.1486	0.98	1.000	6819.879
364128	Sherpa_221_NNPDF30NNLO_Ztautau_MAXHTPTV70_140_CVetoBVeto	e5307_s2726_r7772_r7676_p2949	1981.6000	0.98	0.821	4.982
364129	Sherpa_221_NNPDF30NNLO_Ztautau_MAXHTPTV70_CFilterBVeto	e5307_s2726_r7772_r7676_p2949	1978.8000	0.98	0.113	22.633
364130	Sherpa_221_NNPDF30NNLO_Ztautau_MAXHTPTV70_BFilter	e5307_s2726_r7772_r7676_p2949	1981.8000	0.98	0.064	63.352
364131	Sherpa_221_NNPDF30NNLO_Ztautau_MAXHTPTV70_140_CVetoBVeto	e5307_s2726_r7772_r7676_p2949	110.3700	0.98	0.689	80.065
364132	Sherpa_221_NNPDF30NNLO_Ztautau_MAXHTPTV70_140_CFilterBVeto	e5307_s2726_r7772_r7676_p2949	110.5100	0.98	0.183	99.508
364133	Sherpa_221_NNPDF30NNLO_Ztautau_MAXHTPTV70_140_BFilter	e5307_s2726_r7772_r7676_p2949	110.8700	0.98	0.111	493.213
364134	Sherpa_221_NNPDF30NNLO_Ztautau_MAXHTPTV140_280_CVetoBVeto	e5307_s2726_r7772_r7676_p2949	40.7810	0.98	0.608	204.914
364135	Sherpa_221_NNPDF30NNLO_Ztautau_MAXHTPTV140_280_CFilterBVeto	e5307_s2726_r7772_r7676_p2949	40.7400	0.98	0.229	326.848
364136	Sherpa_221_NNPDF30NNLO_Ztautau_MAXHTPTV140_280_BFilter	e5307_s2726_r7772_r7676_p2949	40.7610	0.98	0.134	923.313
364137	Sherpa_221_NNPDF30NNLO_Ztautau_MAXHTPTV280_500_CVetoBVeto	e5313_s2726_r7772_r7676_p2949	8.5502	0.98	0.560	422.313
364138	Sherpa_221_NNPDF30NNLO_Ztautau_MAXHTPTV280_500_CFilterBVeto	e5313_s2726_r7772_r7676_p2949	8.6707	0.98	0.262	444.352
364139	Sherpa_221_NNPDF30NNLO_Ztautau_MAXHTPTV280_500_BFilter	e5313_s2726_r7772_r7676_p2949	8.6804	0.98	0.173	1347.705
364140	Sherpa_221_NNPDF30NNLO_Ztautau_MAXHTPTV500_1000	e5307_s2726_r7772_r7676_p2949	1.8096	0.98	1.000	1668.876
364141	Sherpa_221_NNPDF30NNLO_Ztautau_MAXHTPTV1000_E_CMS	e5307_s2726_r7772_r7676_p2949	0.1483	0.98	1.000	6775.146

Table A.2: List of simulated Z+jets processes

Dataset ID	Process	Tags	Cross section [pb]	k-factor	Generator efficiency	$\mathcal{L}_{int}[\text{fb}^{-1}]$
410011	PowhegPythiaEvtGen_P2012_singletop_tchan_lept_top	e3824_s2608_s2183_r7725_r7676_p2949	43.7390	1.01	1.000	112.937
410012	PowhegPythiaEvtGen_P2012_singletop_tchan_lept_antitop	e3824_s2608_s2183_r7725_r7676_p2949	25.7780	1.02	1.000	189.903
410015	PowhegPythiaEvtGen_P2012_Wt_dilepton_top	e3753_s2608_s2183_r7725_r7676_p2949	3.5835	1.05	1.000	262.959
410016	PowhegPythiaEvtGen_P2012_Wt_dilepton_antitop	e3753_s2608_s2183_r7725_r7676_p2949	3.5814	1.05	1.000	262.690
410026	PowhegPythiaEvtGen_P2012_SingleTopSchan_noAllHad_antitop	e3998_s2608_s2183_r7725_r7676_p2949	1.2615	1.02	1.000	772.453
410025	PowhegPythiaEvtGen_P2012_SingleTopSchan_noAllHad_top	e3998_s2608_s2183_r7725_r7676_p2949	2.0517	1.00	1.000	484.101

Table A.3: List of simulated single-top processes

Dataset ID	Process	Tags	Cross section [pb]	k-factor	Generator efficiency	$\mathcal{L}_{int}[\text{fb}^{-1}]$
410000	PowhegPythiaEvtGen_P2012_ttbar_hdamp17p5_nonallhad	e3698_s2608_s2183_r7725_r7676_p2949	696.1100	1.19	0.543	109.345

Table A.4: List of the simulated  $t\bar{t}$  sample

Dataset ID	Process	Tags	Cross section [pb]	k-factor	Generator efficiency	$\mathcal{L}_{int}[\text{fb}^{-1}]$
410218	aMcAtNloPythia8EvtGen_MEN30NNLO_A14N23LO_ttee	e5070_s2726_r7772_r7676_p2949	0.0369	1.12	1.000	34099.359
410219	aMcAtNloPythia8EvtGen_MEN30NNLO_A14N23LO_tmmumu	e5070_s2726_r7772_r7676_p2949	0.0369	1.12	1.000	34112.250
410220	aMcAtNloPythia8EvtGen_MEN30NNLO_A14N23LO_tttautau	e5070_s2726_r7772_r7676_p2949	0.0366	1.12	1.000	22792.877
410155	aMcAtNloPythia8EvtGen_MEN30NNLO_A14N23LO_twW	e5070_s2726_r7772_r7676_p2949	0.5483	1.10	1.000	12423.357
410081	MadGraphPythia8EvtGen_A14NNPDF23_ttbarWW	e4111_s2608_s2183_r7725_r7676_p2949	0.0081	1.22	1.000	5048.439
407321	MadGraphPythia8EvtGen_A14NNPDF23LO_ttbarWll	e5536_s2726_r7772_r7676_p2949	0.0003	1.34	1.000	84165.641

Table A.5: List of simulated  $t\bar{t}$  plus vectorboson processes

Dataset ID	Process	Tags	Cross section [pb]	k-factor	Generator efficiency	$\mathcal{L}_{int} [\text{fb}^{-1}]$
341079	PowhegPythia8EvtGen_CTI10_AZNLOCTEQ6L1_ggH125_WWlVv_EF_15_5	e3871_s2608_s2183_r7772_r7676_p2949	0.9902	1.00	0.491	983.382
341122	PowhegPythia8EvtGen_CTI10_AZNLOCTEQ6L1_ggH125_tautauall	e3935_s2608_s2183_r7772_r7676_p2949	1.9081	1.45	0.123	4467.140
341195	PowhegPythia8EvtGen_CTI10_AZNLOCTEQ6L1_ggH125_mumu	e3945_s2608_s2183_r7772_r7676_p2949	0.0066	1.45	1.000	99495.922
342178	PowhegPythia8EvtGen_CTI10_AZNLOCTEQ6L1_ggH125_ee	e4158_s2608_s2183_r7772_r7676_p2949	0.0000	1.45	1.000	293359648.000
341080	PowhegPythia8EvtGen_CTI10_AZNLOCTEQ6L1_VBFH125_WWlVv_EF_15_5	e3871_s2608_s2183_r7772_r7676_p2949	0.0848	1.00	0.510	5774.853
341155	PowhegPythia8EvtGen_CTI10_AZNLOCTEQ6L1_VBFH125_tautauall	e3888_s2608_s2183_r7772_r7676_p2949	0.2420	0.98	0.123	71518.055
341206	PowhegPythia8EvtGen_CTI10_AZNLOCTEQ6L1_VBFH125_mumu	e3945_s2608_s2183_r7772_r7676_p2949	0.0009	0.96	1.000	998280.062
342189	PowhegPythia8EvtGen_CTI10_AZNLOCTEQ6L1_VBFH125_ee	e4158_s2608_s2183_r7772_r7676_p2949	0.0000	0.98	1.000	5208568320.000
342284	Pythia8EvtGen_A14NNPDF23LO_WH125_inc	e4246_s2608_s2183_r7772_r7676_p2949	1.1021	1.25	1.000	72.029
342285	Pythia8EvtGen_A14NNPDF23LO_ZH125_inc	e4246_s2608_s2183_r7772_r7676_p2949	0.6007	1.45	1.000	114.075
341270	aMcAtNloHerwigppEvtGen_UEEE5_CTEQ6L1_CT10ME_ttH125_semilep	e4277_s2608_s2183_r7772_r7676_p2949	0.5085	1.00	0.439	4269.874
341271	aMcAtNloHerwigppEvtGen_UEEE5_CTEQ6L1_CT10ME_ttH125_allhad	e4277_s2608_s2183_r7772_r7676_p2949	0.5085	1.00	0.455	4112.265
341177	aMcAtNloHerwigppEvtGen_UEEE5_CTEQ6L1_CT10ME_ttH125_dil	e4277_s2608_s2183_r7772_r7676_p2949	0.5085	1.00	0.106	35645.684

Table A.6: List of simulated higgs related processes, including Higgs plus vector boson production and  $t\bar{t}H$  processes

Dataset ID	Process	Tags	Cross section [pb]	k-factor	Generator efficiency	$\mathcal{L}_{int} [\text{fb}^{-1}]$
361069	Sherpa_CTI10_llvvjj_ss.EW4	e3836_s2726_r7772_r7676_p2949	0.0258	0.91	1.000	20984.256
361070	Sherpa_CTI10_llvvjj_ss.EW6	e3836_s2608_s2183_r7772_r7676_p2949	0.0434	0.91	1.000	12363.429
361071	Sherpa_CTI10_lllvj_EW6	e3836_s2726_r7772_r7676_p2949	0.0423	0.91	1.000	25415.025
361072	Sherpa_CTI10_llljj_EW6	e3836_s2608_s2183_r7772_r7676_p2949	0.0315	0.91	1.000	2093.411
361073	Sherpa_CTI10_ggllll	e3836_s2608_s2183_r7772_r7676_p2949	0.0210	0.91	1.000	26331.662
361077	Sherpa_CTI10_gglvv	e3836_s2608_s2183_r7772_r7676_p2949	0.8549	0.91	1.000	256.820
363356	Sherpa_221_NNPDF30NNLO_ZqqZll	e5525_s2726_r7772_r7676_p2949	15.5630	1.00	0.140	2447.129
363359	Sherpa_221_NNPDF30NNLO_WpqgWmfv	e5583_s2726_r7772_r7676_p2949	24.7170	1.00	1.000	286.969
363358	Sherpa_221_NNPDF30NNLO_WqqZll	e5525_s2726_r7772_r7676_p2949	3.4370	1.00	1.000	1549.025
363360	Sherpa_221_NNPDF30NNLO_WPqvWmqq	e5983_s2726_r7772_r7676_p2949	112.7400	1.00	1.000	63.110
363489	Sherpa_221_NNPDF30NNLO_WlvZqq	e5525_s2726_r7772_r7676_p2949	11.4130	1.00	1.000	622.098
363490	Sherpa_221_NNPDF30NNLO_llll	e5332_s2726_r7772_r7676_p2949	1.2557	1.00	1.000	14195.509
363491	Sherpa_221_NNPDF30NNLO_lllv	e5332_s2726_r7772_r7676_p2949	4.5877	1.00	1.000	3437.907
363492	Sherpa_221_NNPDF30NNLO_llvv	e5332_s2726_r7772_r7676_p2949	12.4650	1.00	1.000	1187.565

Table A.7: List of simulated diboson processes

Dataset ID	Process	Tags	Cross section [pb]	k-factor	Generator efficiency	$\mathcal{L}_{int} [\text{fb}^{-1}]$
407311	Sherpa_221_NNPDF30NNLO_6l0v_EW6	e5473_s2726_r7772_r7676_p2949	0.0001	1.00	1.000	478749.375
407312	Sherpa_221_NNPDF30NNLO_5l1v_EW6	e5473_s2726_r7772_r7676_p2949	0.0006	1.00	1.000	88080.891
407313	Sherpa_221_NNPDF30NNLO_4l2v_EW6	e5473_s2726_r7772_r7676_p2949	0.0044	1.00	1.000	11216.921
407314	Sherpa_221_NNPDF30NNLO_3l3v_EW6	e5473_s2726_r7772_r7676_p2949	0.0158	1.00	1.000	3029.156
407315	Sherpa_221_NNPDF30NNLO_2l4v_EW6	e5655_s2726_r7772_r7676_p2949	0.0058	1.00	1.000	10108.625

Table A.8: List of simulated triboson processes

Dataset ID	Process	Tags	Cross section [pb]	k-factor	Generator efficiency	$\mathcal{L}_{int} [\text{fb}^{-1}]$
364198	Sherpa_221_NN30NNLO_Zmm_MII10_40_MAXHTPTV0_70_BVeto	e5421_s2726_r7772_r7676_p2949	2413.7000	0.98	0.965	3.270
364199	Sherpa_221_NN30NNLO_Zmm_MII10_40_MAXHTPTV0_70_BFilter	e5421_s2726_r7772_r7676_p2949	2414.7000	0.98	0.034	18.427
364200	Sherpa_221_NN30NNLO_Zmm_MII10_40_MAXHTPTV0_280_BVeto	e5421_s2726_r7772_r7676_p2949	50.3180	0.98	0.892	54.088
364201	Sherpa_221_NN30NNLO_Zmm_MII10_40_MAXHTPTV0_280_BFilter	e5421_s2726_r7772_r7676_p2949	50.2850	0.98	0.102	217.538
364202	Sherpa_221_NN30NNLO_Zmm_MII10_40_MAXHTPTV280_E_CMS_BVeto	e5421_s2726_r7772_r7676_p2949	3.2355	0.98	0.853	220.507
364203	Sherpa_221_NN30NNLO_Zmm_MII10_40_MAXHTPTV280_E_CMS_BFilter	e5421_s2726_r7772_r7676_p2949	3.2800	0.98	0.144	538.250
364204	Sherpa_221_NN30NNLO_Zee_MII10_40_MAXHTPTV0_70_BVeto	e5421_s2726_r7772_r7676_p2949	2415.7000	0.98	0.965	3.253
364205	Sherpa_221_NN30NNLO_Zee_MII10_40_MAXHTPTV0_70_BFilter	e5421_s2726_r7772_r7676_p2949	2416.8999	0.98	0.034	18.605
364206	Sherpa_221_NN30NNLO_Zee_MII10_40_MAXHTPTV0_280_BVeto	e5421_s2726_r7772_r7676_p2949	50.4560	0.98	0.891	54.046
364207	Sherpa_221_NN30NNLO_Zee_MII10_40_MAXHTPTV0_280_BFilter	e5421_s2726_r7772_r7676_p2949	50.4270	0.98	0.109	203.183
364208	Sherpa_221_NN30NNLO_Zee_MII10_40_MAXHTPTV280_E_CMS_BVeto	e5421_s2726_r7772_r7676_p2949	3.2538	0.98	0.854	217.853
364209	Sherpa_221_NN30NNLO_Zee_MII10_40_MAXHTPTV280_E_CMS_BFilter	e5421_s2726_r7772_r7676_p2949	3.2519	0.98	0.145	539.771
364210	Sherpa_221_NN30NNLO_Ztt_MII10_40_MAXHTPTV0_70_BVeto	e5421_s2726_r7772_r7676_p2949	2417.8999	0.98	0.965	3.240
364211	Sherpa_221_NN30NNLO_Ztt_MII10_40_MAXHTPTV0_70_BFilter	e5421_s2726_r7772_r7676_p2949	2414.2000	0.98	0.034	18.720
364212	Sherpa_221_NN30NNLO_Ztt_MII10_40_MAXHTPTV0_280_BVeto	e5421_s2726_r7772_r7676_p2949	50.3700	0.98	0.890	54.057
364213	Sherpa_221_NN30NNLO_Ztt_MII10_40_MAXHTPTV0_280_BFilter	e5421_s2726_r7772_r7676_p2949	50.4400	0.98	0.110	200.586
364214	Sherpa_221_NN30NNLO_Ztt_MII10_40_MAXHTPTV280_E_CMS_BVeto	e5421_s2726_r7772_r7676_p2949	3.2834	0.98	0.851	217.328
364215	Sherpa_221_NN30NNLO_Ztt_MII10_40_MAXHTPTV280_E_CMS_BFilter	e5421_s2726_r7772_r7676_p2949	3.2788	0.98	0.143	530.539

Table A.9: List of simulated drellyan processes

Dataset ID	Process	Tags	Cross section [pb]	k-factor	Generator efficiency	$\mathcal{L}_{int} [\text{fb}^{-1}]$
304014	MadGraphPythia8EvtGen_A14NNPDF23.3top_SM	e4324_a766_a818_r7676_p2949	0.0016	1.00	1.000	121951.219
410080	MadGraphPythia8EvtGen_A14NNPDF23.4topSM	e4111_s2608_s2183_r7725_r7676_p2949	0.0092	1.00	1.000	21607.096

Table A.10: List of simulated multi-top processes

Dataset ID	Process	Tags	Cross section [pb]	k-factor	Generator efficiency	$\mathcal{L}_{int}[\text{fb}^{-1}]$
301535	Sherpa_CTI0_eegammaPt10_35	e3952_s2608_s2183_r7725_r7676_p2949	52.7060	1.00	1.000	94.596
301536	Sherpa_CTI0_mumugammaPt10_35	e3952_s2608_s2183_r7773_r7676_p2949	52.7080	1.00	1.000	94.509
301890	Sherpa_CTI0_enugammaPt35_70	e3952_s2608_s2183_r7725_r7676_p2949	15.3480	1.00	1.000	32.525
301891	Sherpa_CTI0_enugammaPt70_140	e3952_s2608_s2183_r7725_r7676_p2949	1.5282	1.00	1.000	163.591
301892	Sherpa_CTI0_enugammaPt140	e3952_s2608_s2183_r7725_r7676_p2949	0.2415	1.00	1.000	1034.154
301893	Sherpa_CTI0_munugammaPt35_70	e3952_s2608_s2183_r7725_r7676_p2949	15.2720	1.00	1.000	32.674
301894	Sherpa_CTI0_munugammaPt70_140	e3952_s2608_s2183_r7725_r7676_p2949	1.5235	1.00	1.000	163.702
301895	Sherpa_CTI0_munugammaPt140	e3952_s2608_s2183_r7725_r7676_p2949	0.2418	1.00	1.000	1031.303
301896	Sherpa_CTI0_tauaugammaPt35_70	e3952_s2608_s2183_r7725_r7676_p2949	15.2970	1.00	1.000	32.568
301897	Sherpa_CTI0_tauaugammaPt70_140	e3952_s2608_s2183_r7725_r7676_p2949	1.5290	1.00	1.000	163.244
301898	Sherpa_CTI0_tauaugammaPt140	e3952_s2608_s2183_r7725_r7676_p2949	0.2426	1.00	1.000	1028.854
301899	Sherpa_CTI0_eegammaPt35_70	e3952_s2608_s2183_r7725_r7676_p2949	5.2420	1.00	1.000	95.383
301900	Sherpa_CTI0_eegammaPt70_140	e3952_s2608_s2183_r7725_r7676_p2949	0.3846	1.00	1.000	640.749
301901	Sherpa_CTI0_eegammaPt140	e3952_s2608_s2183_r7725_r7676_p2949	0.0472	1.00	1.000	5295.601
301902	Sherpa_CTI0_mumugammaPt35_70	e3952_s2608_s2183_r7725_r7676_p2949	5.2455	1.00	1.000	95.053
301903	Sherpa_CTI0_mumugammaPt70_140	e3952_s2608_s2183_r7725_r7676_p2949	0.3855	1.00	1.000	648.023
301904	Sherpa_CTI0_mumugammaPt140	e3952_s2608_s2183_r7725_r7676_p2949	0.0472	1.00	1.000	5275.190
301905	Sherpa_CTI0_tautaugammaPt35_70	e3952_s2608_s2183_r7725_r7676_p2949	5.2490	1.00	1.000	95.066
301906	Sherpa_CTI0_tautaugammaPt70_140	e3952_s2608_s2183_r7725_r7676_p2949	0.3848	1.00	1.000	649.135
301907	Sherpa_CTI0_tautaugammaPt140	e3952_s2608_s2183_r7725_r7676_p2949	0.0470	1.00	1.000	5295.056

Table A.11: List of simulated  $V+\gamma$  processes

## A.2 List of signal MC samples

Dataset ID	Process	Tags	mass of $\chi_1^\pm/\chi_2^0$	mass of $\chi_1^0$	Cross section [pb]	efficiency
393820	MGPy8EG_A14N23LO_C1N2.Wh.hall_150p0.0p0.2L7	e6153_a766_a821_r7676_p2949	150.0	0.0	5.18088	0.10619
393821	MGPy8EG_A14N23LO_C1N2.Wh.hall_152p5_22p5_2L7	e6153_a766_a821_r7676_p2949	152.5	22.5	4.878938	0.10559
393822	MGPy8EG_A14N23LO_C1N2.Wh.hall_162p5_12p5_2L7	e6153_a766_a821_r7676_p2949	162.5	12.5	3.871788	0.10816
393823	MGPy8EG_A14N23LO_C1N2.Wh.hall_175p0.0p0.2L7	e6153_a766_a821_r7676_p2949	175.0	0.0	2.95327	0.11018
393824	MGPy8EG_A14N23LO_C1N2.Wh.hall_175p0_25p0_2L7	e6153_a766_a821_r7676_p2949	175.0	25.0	2.95327	0.10959
393825	MGPy8EG_A14N23LO_C1N2.Wh.hall_177p5_47p5_2L7	e6153_a766_a821_r7676_p2949	177.5	47.5	2.8037	0.10879
393826	MGPy8EG_A14N23LO_C1N2.Wh.hall_187p5_12p5_2L7	e6153_a766_a821_r7676_p2949	187.5	12.5	2.292682	0.11370
393827	MGPy8EG_A14N23LO_C1N2.Wh.hall_187p5_37p5_2L7	e6153_a766_a821_r7676_p2949	187.5	37.5	2.292682	0.11098
393828	MGPy8EG_A14N23LO_C1N2.Wh.hall_190p0.60p0.2L7	e6153_a766_a821_r7676_p2949	190.0	60.0	2.183638	0.10982
393829	MGPy8EG_A14N23LO_C1N2.Wh.hall_200p0.0p0.2L7	e6153_a766_a821_r7676_p2949	200.0	0.0	1.8074	0.11534
393830	MGPy8EG_A14N23LO_C1N2.Wh.hall_200p0_25p0_2L7	e6153_a766_a821_r7676_p2949	200.0	25.0	1.8074	0.11434
393831	MGPy8EG_A14N23LO_C1N2.Wh.hall_200p0_50p0_2L7	e6153_a766_a821_r7676_p2949	200.0	50.0	1.8074	0.11253
393832	MGPy8EG_A14N23LO_C1N2.Wh.hall_202p5_72p5_2L7	e6153_a766_a821_r7676_p2949	202.5	72.5	1.726133	0.11031
393833	MGPy8EG_A14N23LO_C1N2.Wh.hall_212p5_12p5_2L7	e6153_a766_a821_r7676_p2949	212.5	12.5	1.443136	0.11842
393834	MGPy8EG_A14N23LO_C1N2.Wh.hall_212p5_37p5_2L7	e6153_a766_a821_r7676_p2949	212.5	37.5	1.443136	0.11662
393835	MGPy8EG_A14N23LO_C1N2.Wh.hall_212p5_62p5_2L7	e6153_a766_a821_r7676_p2949	212.5	62.5	1.443136	0.11380
393836	MGPy8EG_A14N23LO_C1N2.Wh.hall_215p0_85p0_2L7	e6153_a766_a821_r7676_p2949	215.0	85.0	1.381487	0.11159
393837	MGPy8EG_A14N23LO_C1N2.Wh.hall_225p0.0p0.2L7	e6153_a766_a821_r7676_p2949	225.0	0.0	1.165122	0.12090
393838	MGPy8EG_A14N23LO_C1N2.Wh.hall_225p0_25p0_2L7	e6153_a766_a821_r7676_p2949	225.0	25.0	1.165122	0.11996
393839	MGPy8EG_A14N23LO_C1N2.Wh.hall_225p0_50p0_2L7	e6153_a766_a821_r7676_p2949	225.0	50.0	1.165122	0.11794
393840	MGPy8EG_A14N23LO_C1N2.Wh.hall_225p0_75p0_2L7	e6153_a766_a821_r7676_p2949	225.0	75.0	1.165122	0.11487
393841	MGPy8EG_A14N23LO_C1N2.Wh.hall_227p5_97p5_2L7	e6153_a766_a821_r7676_p2949	227.5	97.5	1.118027	0.11211
393842	MGPy8EG_A14N23LO_C1N2.Wh.hall_237p5_12p5_2L7	e6153_a766_a821_r7676_p2949	237.5	12.5	0.950655	0.12238
393843	MGPy8EG_A14N23LO_C1N2.Wh.hall_237p5_37p5_2L7	e6153_a766_a821_r7676_p2949	237.5	37.5	0.950655	0.12171
393844	MGPy8EG_A14N23LO_C1N2.Wh.hall_237p5_62p5_2L7	e6153_a766_a821_r7676_p2949	237.5	62.5	0.950655	0.11997
393845	MGPy8EG_A14N23LO_C1N2.Wh.hall_237p5_87p5_2L7	e6153_a766_a821_r7676_p2949	237.5	87.5	0.950655	0.11401
393846	MGPy8EG_A14N23LO_C1N2.Wh.hall_240p0_110p0_2L7	e6153_a766_a821_r7676_p2949	240.0	110.0	0.913692	0.11273
393847	MGPy8EG_A14N23LO_C1N2.Wh.hall_250p0_0p0.2L7	e6153_a766_a821_r7676_p2949	250.0	0.0	0.782514	0.12732
393848	MGPy8EG_A14N23LO_C1N2.Wh.hall_250p0_25p0_2L7	e6153_a766_a821_r7676_p2949	250.0	25.0	0.782514	0.12395
393849	MGPy8EG_A14N23LO_C1N2.Wh.hall_250p0_50p0_2L7	e6153_a766_a821_r7676_p2949	250.0	50.0	0.782514	0.12211
393850	MGPy8EG_A14N23LO_C1N2.Wh.hall_250p0_75p0_2L7	e6153_a766_a821_r7676_p2949	250.0	75.0	0.782514	0.12087
393851	MGPy8EG_A14N23LO_C1N2.Wh.hall_250p0_100p0_2L7	e6153_a766_a821_r7676_p2949	250.0	100.0	0.782514	0.11736
393852	MGPy8EG_A14N23LO_C1N2.Wh.hall_262p5_12p5_2L7	e6153_a766_a821_r7676_p2949	262.5	12.5	0.649397	0.12647
393853	MGPy8EG_A14N23LO_C1N2.Wh.hall_262p5_37p5_2L7	e6153_a766_a821_r7676_p2949	262.5	37.5	0.649397	0.12603
393854	MGPy8EG_A14N23LO_C1N2.Wh.hall_262p5_62p5_2L7	e6153_a766_a821_r7676_p2949	262.5	62.5	0.649397	0.12457
393855	MGPy8EG_A14N23LO_C1N2.Wh.hall_262p5_87p5_2L7	e6153_a766_a821_r7676_p2949	262.5	87.5	0.649397	0.12131
393856	MGPy8EG_A14N23LO_C1N2.Wh.hall_275p0_0p0.2L7	e6153_a766_a821_r7676_p2949	275.0	0.0	0.54305	0.12896
393857	MGPy8EG_A14N23LO_C1N2.Wh.hall_275p0_25p0_2L7	e6153_a766_a821_r7676_p2949	275.0	25.0	0.54305	0.12850
393858	MGPy8EG_A14N23LO_C1N2.Wh.hall_275p0_50p0_2L7	e6153_a766_a821_r7676_p2949	275.0	50.0	0.54305	0.12794
393859	MGPy8EG_A14N23LO_C1N2.Wh.hall_275p0_75p0_2L7	e6153_a766_a821_r7676_p2949	275.0	75.0	0.54305	0.12526
393860	MGPy8EG_A14N23LO_C1N2.Wh.hall_287p5_12p5_2L7	e6153_a766_a821_r7676_p2949	287.5	12.5	0.456978	0.13264
393861	MGPy8EG_A14N23LO_C1N2.Wh.hall_287p5_37p5_2L7	e6153_a766_a821_r7676_p2949	287.5	37.5	0.456978	0.12975
393862	MGPy8EG_A14N23LO_C1N2.Wh.hall_287p5_62p5_2L7	e6153_a766_a821_r7676_p2949	287.5	62.5	0.456978	0.12952
393863	MGPy8EG_A14N23LO_C1N2.Wh.hall_300p0_0p0.2L7	e6153_a766_a821_r7676_p2949	300.0	0.0	0.386946	0.13283
393864	MGPy8EG_A14N23LO_C1N2.Wh.hall_300p0_25p0_2L7	e6153_a766_a821_r7676_p2949	300.0	25.0	0.386946	0.13473
393865	MGPy8EG_A14N23LO_C1N2.Wh.hall_300p0_50p0_2L7	e6153_a766_a821_r7676_p2949	300.0	50.0	0.386946	0.13213
393866	MGPy8EG_A14N23LO_C1N2.Wh.hall_300p0_75p0_2L7	e6153_a766_a821_r7676_p2949	300.0	75.0	0.386946	0.12999
393867	MGPy8EG_A14N23LO_C1N2.Wh.hall_300p0_100p0_2L7	e6153_a766_a821_r7676_p2949	300.0	100.0	0.386946	0.12741
393868	MGPy8EG_A14N23LO_C1N2.Wh.hall_312p5_12p5_2L7	e6153_a766_a821_r7676_p2949	312.5	12.5	0.329476	0.13550
393869	MGPy8EG_A14N23LO_C1N2.Wh.hall_312p5_37p5_2L7	e6153_a766_a821_r7676_p2949	312.5	37.5	0.329476	0.13478
393870	MGPy8EG_A14N23LO_C1N2.Wh.hall_325p0_0p0.2L7	e6153_a766_a821_r7676_p2949	325.0	0.0	0.281924	0.13702
393871	MGPy8EG_A14N23LO_C1N2.Wh.hall_325p0_25p0_2L7	e6153_a766_a821_r7676_p2949	325.0	25.0	0.281924	0.13792
393872	MGPy8EG_A14N23LO_C1N2.Wh.hall_325p0_50p0_2L7	e6153_a766_a821_r7676_p2949	325.0	50.0	0.281924	0.13644
393873	MGPy8EG_A14N23LO_C1N2.Wh.hall_325p0_75p0_2L7	e6153_a766_a821_r7676_p2949	325.0	75.0	0.281924	0.13477
393874	MGPy8EG_A14N23LO_C1N2.Wh.hall_325p0_100p0_2L7	e6153_a766_a821_r7676_p2949	325.0	100.0	0.281924	0.13162
393875	MGPy8EG_A14N23LO_C1N2.Wh.hall_337p5_12p5_2L7	e6153_a766_a821_r7676_p2949	337.5	12.5	0.24248	0.14099
393876	MGPy8EG_A14N23LO_C1N2.Wh.hall_350p0_0p0.2L7	e6153_a766_a821_r7676_p2949	350.0	0.0	0.209458	0.14094
393877	MGPy8EG_A14N23LO_C1N2.Wh.hall_350p0_25p0_2L7	e6153_a766_a821_r7676_p2949	350.0	25.0	0.209458	0.14240
393878	MGPy8EG_A14N23LO_C1N2.Wh.hall_350p0_50p0_2L7	e6153_a766_a821_r7676_p2949	350.0	50.0	0.209458	0.14057
393879	MGPy8EG_A14N23LO_C1N2.Wh.hall_350p0_75p0_2L7	e6153_a766_a821_r7676_p2949	350.0	75.0	0.209458	0.14114
393880	MGPy8EG_A14N23LO_C1N2.Wh.hall_350p0_100p0_2L7	e6153_a766_a821_r7676_p2949	350.0	100.0	0.209458	0.13746
393881	MGPy8EG_A14N23LO_C1N2.Wh.hall_375p0_0p0.2L7	e6153_a766_a821_r7676_p2949	375.0	0.0	0.158076	0.14497
393882	MGPy8EG_A14N23LO_C1N2.Wh.hall_375p0_25p0_2L7	e6153_a766_a821_r7676_p2949	375.0	25.0	0.158076	0.14609
393883	MGPy8EG_A14N23LO_C1N2.Wh.hall_375p0_50p0_2L7	e6153_a766_a821_r7676_p2949	375.0	50.0	0.158076	0.14322
393884	MGPy8EG_A14N23LO_C1N2.Wh.hall_375p0_75p0_2L7	e6153_a766_a821_r7676_p2949	375.0	75.0	0.158076	0.14262
393885	MGPy8EG_A14N23LO_C1N2.Wh.hall_400p0_0p0.2L7	e6153_a766_a821_r7676_p2949	400.0	0.0	0.121027	0.15012
393886	MGPy8EG_A14N23LO_C1N2.Wh.hall_400p0_25p0_2L7	e6153_a766_a821_r7676_p2949	400.0	25.0	0.121027	0.14731
393887	MGPy8EG_A14N23LO_C1N2.Wh.hall_400p0_50p0_2L7	e6153_a766_a821_r7676_p2949	400.0	50.0	0.121027	0.14735
393888	MGPy8EG_A14N23LO_C1N2.Wh.hall_400p0_75p0_2L7	e6153_a766_a821_r7676_p2949	400.0	75.0	0.121027	0.14707
393889	MGPy8EG_A14N23LO_C1N2.Wh.hall_400p0_100p0_2L7	e6153_a766_a821_r7676_p2949	400.0	100.0	0.121027	0.14600
393890	MGPy8EG_A14N23LO_C1N2.Wh.hall_425p0_0p0.2L7	e6153_a766_a821_r7676_p2949	425.0	0.0	0.093788	0.15456
393891	MGPy8EG_A14N23LO_C1N2.Wh.hall_425p0_25p0_2L7	e6153_a766_a821_r7676_p2949	425.0	25.0	0.093788	0.15310
393892	MGPy8EG_A14N23LO_C1N2.Wh.hall_425p0_50p0_2L7	e6153_a766_a821_r7676_p2949	425.0	50.0	0.093788	0.15361
393893	MGPy8EG_A14N23LO_C1N2.Wh.hall_425p0_75p0_2L7	e6153_a766_a821_r7676_p2949	425.0	75.0	0.093788	0.15161
393894	MGPy8EG_A14N23LO_C1N2.Wh.hall_425p0_100p0_2L7	e6153_a766_a821_r7676_p2949	425.0	100.0	0.093788	0.14988
393895	MGPy8EG_A14N23LO_C1N2.Wh.hall_475p0_0p0.2L7	e6153_a766_a821_r7676_p2949	475.0	0.0	0.073446	0.15549
393896	MGPy8EG_A14N23LO_C1N2.Wh.hall_475p0_25p0_2L7	e6153_a766_a821_r7676_p2949	475.0	25.0	0.073446	0.15494
393897	MGPy8EG_A14N23LO_C1N2.Wh.hall_475p0_50p0_2L7	e6153_a766_a821_r7676_p2949	475.0	50.0	0.073446	0.15682
393898	MGPy8EG_A14N23LO_C1N2.Wh.hall_475p0_75p0_2L7	e6153_a766_a821_r7676_p2949	475.0	75.0	0.073446	0.15568
393899	MGPy8EG_A14N23LO_C1N2.Wh.hall_475p0_100p0_2L7	e6153_a766_a821_r7676_p2949	475.0	100.0	0.073446	0.15442
393900	MGPy8EG_A14N23LO_C1N2.Wh.hall_475p0_125p0_2L7	e6153_a766_a821_r7676_p2949	475.0	0.0	0.058091	0.16055
393901	MGPy8EG_A14N23LO_C1N2.Wh.hall_475p0_175p0_2L7	e6153_a766_a821_r7676_p2949	475.0	25.0	0.058091	0.16178
393902	MGPy8EG_A14N23LO_C1N2.Wh.hall_475p0_225p0_2L7	e6153_a766_a821_r7676_p2949	475.0	50.0	0.058091	0.16086
393903	MGPy8EG_A14N23LO_C1N2.Wh.hall_475p0_275p0_2L7	e6153_a766_a821_r7676_p2949	475.0	75.0	0.058091	0.15701
393904	MGPy8EG_A14N23LO_C1N2.Wh.hall_475p0_100p0_2L7	e6153_a766_a821_r7676_p2949	475.0	100.0	0.058091	0.16078
393905	MGPy8EG_A14N23LO_C1N2.Wh.hall_500p0_0p0.2L7	e6153_a766_a821_r7676_p2949	500.0	0.0	0.046357	0.16288
393906	MGPy8EG_A14N23LO_C1N2.Wh.hall_500p0_25p0_2L7	e6153_a766_a821_r7676_p2949	500.0	25.0	0.046357	0.16494
393907	MGPy8EG_A14N23LO_C1N2.Wh.hall_500p0_					



# References

- [1] *Standard Model of Elementary Particles*,  
[https://en.wikipedia.org/wiki/File:Standard\\_Model\\_of\\_Elementary\\_Particles.svg](https://en.wikipedia.org/wiki/File:Standard_Model_of_Elementary_Particles.svg).
- [2] *Standard Model Feynman Diagram Vertices*,  
[https://en.wikipedia.org/wiki/File:Standard\\_Model\\_Feynman\\_Diagram\\_Vertices.png](https://en.wikipedia.org/wiki/File:Standard_Model_Feynman_Diagram_Vertices.png).
- [3] E. Mobs, *The CERN accelerator complex. Complexe des accélérateurs du CERN*, <https://cds.cern.ch/record/2197559>, General Photo.
- [4] J. Pequenao, *Computer generated image of the whole ATLAS detector*,  
<https://cds.cern.ch/record/1095924>.
- [5] J. Pequenao and P. Schaffner, *An computer generated image representing how ATLAS detects particles*, <https://cds.cern.ch/record/1505342>.
- [6] J. Pequenao, *Computer generated image of the ATLAS inner detector*,  
<https://cds.cern.ch/record/1095926>.
- [7] G. Aad, E. Abat, and J. Abdallah, *The ATLAS Experiment at the CERN Large Hadron Collider*, Journal of Instrumentation **3** (2008) S08003,  
<http://stacks.iop.org/1748-0221/3/i=08/a=S08003>.
- [8] J. Pequenao, *Computer Generated image of the ATLAS calorimeter*,  
<https://cds.cern.ch/record/1095927>.
- [9] J. Pequenao, *Computer generated image of the ATLAS Muons subsystem*,  
<https://cds.cern.ch/record/1095929>.
- [10] *The accelerator complex*, <https://home.cern/about/accelerators>.

- [11] *Pulling together: Superconducting electromagnets*,  
[https://home.cern/about/engineering/  
pulling-together-superconducting-electromagnets.](https://home.cern/about/engineering/pulling-together-superconducting-electromagnets)
- [12] *Cryogenics: Low temperatures, high performance*, [https://home.cern/  
about/engineering/cryogenics-low-temperatures-high-performance.](https://home.cern/about/engineering/cryogenics-low-temperatures-high-performance)